



Coupled modelling of hydrological processes and grassland production in two contrasting climates

^{1*}Nicholas Jarvis, ^{2,3}Jannis Groh, ¹Elisabet Lewan, ¹Katharina H. E. Meurer, ⁴Walter Durka,
⁴Cornelia Baessler⁴, ²Thomas Pütz, ¹Elvin Ruffullayev, ²Harry Vereecken

¹*Soil and Environment, Swedish University of Agricultural Sciences, Uppsala, Sweden*

²*Agrosphere (IBG-3), Institute of Bio- and Geoscience, Forschungszentrum Jülich GmbH, Jülich, Germany*

³*Research Area 1 "Landscape Functioning", Working Group "Hydropedology", Leibniz Centre for Agricultural Landscape Research (ZALF), Müncheberg, Germany*

⁴*Department of Community Ecology (BZF), Helmholtz Centre for Environmental Research (UFZ), Halle, Germany*

*corresponding author (nicholas.jarvis@slu.se)



1 Abstract

2 Projections of global climate models suggest that ongoing human-induced climate change will
3 lead to an increase in the frequency of severe droughts in many important agricultural regions
4 of the world. Eco-hydrological models that integrate current understanding of the interacting
5 processes governing soil water balance and plant growth may be useful tools to predict the
6 impacts of climate change on crop production. However, the validation status of these models
7 for making predictions under climate change is still unclear, since few suitable datasets are
8 available for model testing. One promising approach is to test models using data obtained in
9 “space-for-time” substitution experiments, in which samples are transferred among locations
10 with contrasting current climates in order to mimic future climatic conditions. An important
11 advantage of this approach is that the soil type is the same, so that differences in soil
12 properties are not confounded with the influence of climate on water balance and crop
13 growth. In this study, we evaluate the capability of a relatively simple eco-hydrological model
14 to reproduce 6 years (2013-2018) of measurements of soil water contents, water balance
15 components and grass production made in weighing lysimeters located at two sites within the
16 TERENO-SoilCan network in Germany. Three lysimeters are located at an upland site at
17 Rollesbroich with a cool, wet climate, while three others had been moved from Rollesbroich
18 to a warmer and drier climate on the lower Rhine valley floodplain at Selhausen. Four of the
19 most sensitive parameters in the model were treated as uncertain within the framework of
20 the GLUE (Generalized Likelihood Uncertainty Estimation) methodology, while the remaining
21 parameters in the model were set according to site measurements or data in the literature.

22 The model accurately reproduced the measurements at both sites, and some significant
23 differences in the posterior ranges of the four uncertain parameters were found. In particular,
24 the results indicated greater stomatal conductance as well an increase in dry matter allocation
25 below-ground and a significantly larger maximum root depth for the three lysimeters that had
26 been moved to Selhausen. As a consequence, the apparent water use efficiency (above-
27 ground harvest divided by evapotranspiration) was significantly smaller at Selhausen than
28 Rollesbroich. Data on species abundance on the lysimeters provide one possible explanation
29 for the differences in the plant traits at the two sites derived from model calibration. These
30 observations showed that the plant community at Selhausen had changed significantly in
31 response to the drier climate, with a significant decrease in the abundance of herbs and an
32 increase in the proportion of grass species. The differences in root depth and leaf conductance
33 may also be a consequence of plasticity or acclimation at the species level. Regardless of the
34 reason, we may conclude that such adaptations introduce significant additional uncertainties
35 into model predictions of water balance and plant growth in response to climate change.



36 1. Introduction

37 Projections of global climate models suggest that ongoing human-induced climate change will
38 lead to an increase in the frequency of severe droughts (Ruane et al., 2018). This may seriously
39 impact production in many important agricultural regions of the world (Tubiello et al., 2007),
40 including managed grasslands (e.g. Kipling et al., 2016; Stanimirova et al., 2019), since key
41 forage species are known to be sensitive to drought (Norris, 1982; Coleman et al., 1989;
42 Silvertown et al., 1994; Jenkinson et al., 1994; Volaire et al., 1998; Meurer et al., 2019).
43 Grasslands are also of major importance in the context of climate change mitigation, since
44 they cover ca. 70% of the global agricultural land area (Foley et al., 2011) and represent a large
45 store of soil organic carbon (SOC) (Li et al., 2018; Bossio et al., 2020). Soil water status affects
46 plant growth through a complex web of direct and indirect mechanisms (Körner, 2015; White
47 et al., 2016; Tardieu et al., 2018; Loka et al., 2019; Gupta et al., 2020). In turn, plant growth,
48 both above- and below-ground, influences the soil water balance through important feedback
49 mechanisms, particularly the regulation of transpiration by leaf area as well as the control of
50 water supply from the soil by root length density and its distribution with depth (Monteith,
51 1986, 1988; Tardieu et al., 2017). Thus, realistic models of the coupled processes of root water
52 uptake, transpiration and plant growth are required to predict reliably the impacts of climate
53 change on the future productive potential of grassland. Eco-hydrological models that attempt
54 to capture these interactions in the soil-plant system are widely used in climate change studies
55 that focus on the prediction of latent and sensible heat fluxes and CO₂ exchange between the
56 land surface and the atmosphere (e.g. Fatichi et al., 2016; Klein et al., 2017; Kellner et al.,
57 2017). Similarly, soil-crop models that integrate current understanding of the interacting
58 processes governing water balance, SOC and nutrient cycling and crop growth (e.g. Robertson
59 et al., 2015; Wu et al., 2016; Stöckle and Kemanian, 2020) are often used as tools to predict
60 the impacts of land use or climate change on crop production and the environment (e.g.
61 Eckersten et al., 2012). These two types of simulation model share many similarities. In the
62 following, we refer to them collectively as SVAT (soil-vegetation-atmosphere) models.

63 SVAT models employ empirical (or phenomenological) approaches to describe many of the
64 key processes in the soil-plant system. This is especially the case for the processes governing
65 plant growth because the underlying mechanisms are extremely complex and not easily
66 amenable to fundamental descriptions (Boote et al., 2013; Wu et al., 2016). This means that
67 great care is needed in model calibration exercises, given the usual paucity of experimental
68 data in relation to the number of model parameters. In such cases, parameter errors may
69 often compensate for model deficiencies leading to non-unique solutions or ‘equifinality’
70 (Beven and Binley, 1992; Beven, 2006). Parameter uncertainty has not always been
71 considered in SVAT model applications (Seidel et al., 2018). Thus, even though a model
72 performs satisfactorily, it may be doing so for the wrong reasons (Kirchner, 2006). As a
73 consequence, model predictions, for example for a future climate, can be seriously in error
74 (Kersebaum et al., 2007, 2015; Bellocchi et al., 2010; He et al., 2017). In this respect, despite
75 their great potential, it is not yet clear how accurately SVAT models can predict the soil water
76 balance and production potential of grasslands in a changing climate because few suitably
77 comprehensive data sets have been available to unequivocally constrain them in model
78 calibration exercises. Several SVAT models specifically designed for grassland agro-ecosystems



79 have been developed (e.g. Joven et al., 2006a,b; Jing et al., 2012; Persson et al., 2014).
80 However, with only a few exceptions, previous studies have focused on calibrating these
81 models against data on above-ground biomass production at single sites, with scant focus on
82 hydrological processes and below-ground biomass, and with little attention paid to parameter
83 uncertainty. In a test of the *PaSim* grassland model at the regional scale, Ma et al. (2015) found
84 that although CO₂ and water fluxes between the land surface and atmosphere were
85 reasonably well matched, soil water contents were not accurately simulated during dry
86 periods. Similarly, in a multi-model and multi-site validation exercise, Sándor et al. (2017)
87 noted a variable model performance at sites with contrasting climates. In particular, they
88 demonstrated a failure of the models to simulate correctly root water uptake patterns and
89 biomass production in dry summers and at dry sites. Even though most grassland species are
90 generally comparatively shallow-rooted (Jackson et al., 1996), several previous studies have
91 highlighted the role of sparsely distributed deeper roots in maintaining water uptake,
92 transpiration and growth during droughts (e.g. Kemp and Culvenor, 1994; Volaire et al 1998;
93 Bonos and Murphy, 1999; Zwicke et al., 2015). This suggests that models of root water uptake
94 for grass must account for compensatory mechanisms, whereby water uptake increases from
95 sparsely rooted wetter soil layers to compensate for reductions in water uptake in densely
96 rooted, but dry soil (Jarvis, 2011; Cai et al., 2017).

97 Manipulation experiments have been carried out to simulate the effects of climate change on
98 grasslands in which plant growth has been monitored following controlled alterations in the
99 precipitation regime (e.g. reduced rainfall amount or frequency). However, nearly all of these
100 experiments are of a short-term nature and the treatments imposed have often been extreme
101 and thus not well adapted to climate model projections (e.g. Beier et al., 2012; Hoover et al.,
102 2018). Furthermore, with only a few exceptions (e.g. Bollig and Feller, 2014), drought
103 manipulation experiments have not focused much on the complex interactions between soil
104 hydrological processes, water stress and plant growth, despite their importance. Thus, in most
105 cases, the mechanisms controlling the observed growth responses have not been elucidated
106 in detail, while little data is available from these experiments that could support and test
107 model predictions (Beier et al., 2012; Hoover et al., 2018). An alternative approach is to test
108 model performance against data obtained in “space-for-time” substitution experiments, in
109 which samples are transferred among sites with contrasting current climates in order to
110 approximately mimic likely future climate conditions (Ineson et al., 1998; Pütz et al., 2016).
111 One important advantage of this approach is that the soil type is the same, so that differences
112 in soil properties are not confounded with the influence of climate on soil hydrology and crop
113 growth. Weighing lysimeters are highly suitable study objects in this context, since they enable
114 the measurement of a complete (closed) water balance (Wegehenkel et al., 2008; Heinlein et
115 al., 2017; Groh et al., 2020a). Providing they are sufficiently large in terms of both depth and
116 diameter, weighing lysimeters also represent a relatively natural environment for plant
117 growth as well as allowing the installation of instrumentation to measure soil water status.

118 In this study, we make use of data from the TERENO-SoilCan network, in which large weighing
119 lysimeters containing undisturbed soil monoliths have been transferred among several
120 locations in Germany to emulate expected changes in climate (Zacharias et al., 2011; Pütz et
121 al., 2016; Groh et al., 2020b). In this study, we evaluate the capability of a relatively simple



122 eco-hydrological model to reproduce six years of measurements of the soil water balance and
123 grassland production in lysimeters at two sites in the Eifel/Lower Rhine Valley observatory
124 (Zacharias et al., 2011; Pütz et al., 2016; Bogena et al., 2018). Three of these lysimeters are
125 located at an upland site at Rollesbroich with a cool, wet climate, while three others were
126 moved from Rollesbroich to a warmer, drier climate in the Rhine valley at Selhausen.

127 2. Materials and methods

128 2.1 Site descriptions, vegetation, soil properties and lysimeter data

129 The station at Rollesbroich (50° 37' N, 6° 18' E) is located on a hilltop site at an elevation of
130 511 m, while Selhausen (50° 52' N, 6° 27' E) is located on a relatively flat alluvial flood plain in
131 the lower Rhine valley at an altitude of 104 m. The mean annual air temperature at
132 Rollesbroich is 8°C and the mean annual precipitation is 1150 mm. At Selhausen, the mean
133 annual air temperature is 10°C and the mean annual precipitation is 720 mm. A weather
134 station at each site records precipitation, solar radiation, air temperature, air humidity and
135 wind speed at a height of 2 m at a ten-minute time resolution (Pütz et al., 2016), which we
136 aggregated to a daily time step. From these meteorological variables, we calculated daily
137 reference (potential) evapotranspiration for grass with the FAO Penman-Monteith equation
138 (Allen et al., 1998) as a simple comparative measure of the atmospheric demand for water in
139 the two climates. The meteorological data and calculated reference evapotranspiration at the
140 two sites for the period 2013-2018 are shown in the supplementary information (figure S1).

141 The soil at Rollesbroich is a Stagnic Cambisol, with the basic properties shown in Table 1. The
142 soil is a sandy loam in the topsoil, changing abruptly to a clay loam at 24 cm depth. The texture
143 again becomes coarser (sandy loam/loam) in the deep subsoil below 93 cm (Table 1). The
144 original grassland community on the lysimeters extracted at Rollesbroich is classified as a
145 mesic grassland of the Arrhenatheretalia alliance without any clear affiliation to classical plant
146 associations. The community is dominated by *Lolium perenne* L., *Ranunculus repens* L., *Rumex*
147 *acetosa* L., *Taraxacum officinale* L., *Dactylis glomerata* L. and *Trifolium repens* L. During the
148 extraction of the lysimeters at Rollesbroich, grassland roots were observed to extend to ca.
149 40-50 cm depth (J. Groh, T. Pütz, pers. comm.). This is supported by SOC contents measured
150 in the soil profile, which decline abruptly below 50 cm depth (Table 1). The lysimeters are
151 supplied with fertilizer as liquid manure and the vegetation is cut 3 to 4 times per growing
152 season to characterize above-ground biomass production, following the local management
153 practice. During the first four years (2013-2016) of the experimental period, leaf area index
154 was measured on multiple occasions with an LAI-2200C Plant Canopy Analyzer from Licor.
155 Plant height was also measured using a conventional ruler. Plant communities present in the
156 lysimeters were assessed annually during the period 2011 to 2016. Plant species abundance
157 was estimated as the number of grid cells occupied of 64 rectangular cells (10 × 10cm). Based
158 on this data, the relative abundances of three plant functional types (i.e. grasses, legumes and
159 non-legume herbs) were quantified. These observations showed that plant communities
160 changed significantly at both sites, with a general decrease in the abundance of herbs and an
161 increase in the proportion of grass species (figure S2). This change was much less pronounced
162 at Rollesbroich than in the lysimeters transferred to Selhausen, where the plant community



163 composition diverged continuously from the original resident community composition,
164 presumably in response to the move to the warmer and drier climate. The small changes in
165 community composition found at Rollesbroich may be a consequence of the experimental set-
166 up. For example, the lysimeters do not allow for root-ingrowth of rhizomatous herb species.

167 The lysimeters have a surface area of 1 m² and are 1.5 m deep. Weighing devices (load cells)
168 measure weight changes equivalent to a water depth of 0.01 mm. Application of a filter
169 routine to separate signal from noise enables accurate estimations of both precipitation and
170 evapotranspiration from each lysimeter (Peters et al., 2017). Missing precipitation data were
171 filled in a first step using the mean value calculated for all available lysimeters. In a second
172 step, any remaining gaps were then filled using the precipitation measured by the reference
173 precipitation gauge. Water fluxes into and out of the lysimeters at the base are controlled by
174 measurements of soil water pressure heads made in the surrounding soil at 1.4 m depth. Soil
175 water contents and pressure heads are measured at a ten-minute time resolution at three
176 depths (10, 30 and 50 cm depth) in the lysimeters using TDR probes and tensiometers (30 and
177 50 cm depth) or matric potential sensors (10 cm depth). A detailed description of the design,
178 construction and extraction of the lysimeters and their installation in the lysimeter stations of
179 the SoilCan network can be found in Pütz et al. (2016). Three lysimeters were moved from
180 Rollesbroich to Selhausen in November 2011. In this study, we make use of measurements
181 made in a six-year period from 2013 to 2018.

182 Table 2 summarizes the annual average water balances measured in the six lysimeters in the
183 six-year period from 2013 to 2018, as well as the average annual harvested biomass and
184 calculations of the water use efficiency, defined as the ratio of harvest to evapotranspiration.
185 In the wet climate at Rollesbroich, actual evapotranspiration was ca. 90% of the potential rate
186 calculated by the FAO version of the Penman-Monteith equation for the period 2013-2018
187 (641 and 710 mm/year respectively), while percolation from the lysimeters was on average
188 42% of the precipitation (442 and 1062 mm/year respectively). Thus, evapotranspiration at
189 Rollesbroich is mostly limited by the available energy and is only rarely limited by water supply
190 (Gebler et al., 2015; Rahmati et al., 2020). Notably, the ratio of actual to potential
191 evapotranspiration was only slightly smaller in the much drier climate of Selhausen than at
192 Rollesbroich (on average 86%, Table 2). Figure 1 shows that a strong limitation of the water
193 supply on evapotranspiration at Selhausen can only be seen in the very dry year of 2018, when
194 the ratio between actual and potential rates fell to ca. 60%. It is also striking that the actual
195 evapotranspiration slightly exceeds precipitation at Selhausen, so that the net percolation at
196 the base of the lysimeters is negative (i.e. an upwards directed flow; Table 2).

197 Table 2 shows that the differences in water balance components among the three replicate
198 lysimeters at both sites are very small. For precipitation, the difference between the largest
199 and smallest measured totals among the replicates at Rollesbroich and Selhausen is only ca.
200 3% and 1% of the mean value respectively. Furthermore, the difference in evapotranspiration
201 between the two lysimeters with the largest and smallest values is equivalent to only 1% of
202 the precipitation at Selhausen and 2.6% of the precipitation at Rollesbroich. This limited
203 within-site variation in hydrologic response appears to be consistent with the available data
204 for soil water contents and pressure heads. The ‘in situ’ water retention data (Figure S3 and



205 Table S1) suggest that there is limited spatial variation in soil hydraulic properties among the
 206 six lysimeters. Percolation is somewhat more variable (Table 2), despite the fact that the
 207 pressure heads in the surrounding soil at 1.4 m depth controlling water flow at the base of the
 208 lysimeter are also quite similar among the replicates, especially at Rollesbroich (see figure S4).

209 Likewise, harvested biomass at Selhausen was similar in all three replicate lysimeters, whereas
 210 it varied more at Rollesbroich, with one lysimeter clearly an outlier (Ro_Y_013, Table 2). Much
 211 larger nitrate nitrogen concentrations were consistently found at the beginning of the
 212 experiment in the leachate from this lysimeter (Giraud et al. 2021), which suggests that the
 213 larger harvest from Ro_Y_013 may be due to a better nutrient supply from the soil. Table 2
 214 and figure 2 show that the water use efficiency (WUE) of the grassland in the drier climate at
 215 Selhausen was smaller than for the lysimeters at Rollesbroich (Forstner et al., 2021), since
 216 harvests were somewhat smaller and evapotranspiration was larger.

217 In the following, we assess the capability of a relatively simple (parsimonious) eco-hydrological
 218 model to match the data measured in the replicate lysimeters in the two contrasting climates
 219 at Rollesbroich and Selhausen. We also use the model to identify plausible reasons for the
 220 differences in soil hydrology and grassland growth observed between the sites.

221 2.2 Model description

222 2.2.1 Potential evapotranspiration

223 In the longer term, the extent of grass cover can be affected by a changing climate, which will
 224 alter the energy balance partitioning at the land surface. We therefore employ the dual-source
 225 Penman-Monteith equation (Shuttleworth and Wallace, 1985; Shuttleworth and Gurney,
 226 1990), which enables the estimation of potential soil evaporation E_p (m day⁻¹) and potential
 227 transpiration T_p (m day⁻¹) from dynamic plant properties and meteorological variables:

$$228 \quad E_p = \frac{C_s}{\lambda} \left[\frac{\Delta R_n + \left\{ \frac{\rho c_p VPD - \Delta r_a^s (R_n - R_{n(s)})}{r_a^a + r_a^s} \right\}}{\Delta + \gamma \left(1 + \left(\frac{r_s^s}{r_a^a + r_a^c} \right) \right)} \right] \quad (1)$$

$$229 \quad T_p = \frac{C_c}{\lambda} \left\{ \frac{\Delta R_n + \left\{ \frac{\rho c_p VPD - \Delta r_a^c R_{n(s)}}{r_a^a + r_a^c} \right\}}{\Delta + \gamma \left(1 + \left(\frac{r_s^c}{r_a^a + r_a^c} \right) \right)} \right\} \quad (2)$$

$$230 \quad C_s = \frac{1}{1 + \left(\frac{R_s R_a}{R_c (R_s + R_a)} \right)} \quad (3)$$

$$231 \quad C_c = \frac{1}{1 + \left(\frac{R_c R_a}{R_s (R_c + R_a)} \right)} \quad (4)$$

$$232 \quad R_a = (\Delta + \gamma) r_a^a \quad (5)$$

$$233 \quad R_c = (\Delta + \gamma) r_a^c + \gamma r_s^c \quad (6)$$

$$234 \quad R_s = (\Delta + \gamma) r_a^s + \gamma r_s^s \quad (7)$$



235 where λ is the latent heat of vapourisation, ρ is the air density, C_p is the specific heat of air,
236 VPD is the vapour pressure deficit, Δ is the slope of the saturation vapour pressure curve, γ is
237 the psychrometer constant, r_s^s is the surface resistance of wet soil (here fixed at 20 s m^{-1}), r_s^c
238 and r_a^c are the bulk unstressed stomatal and boundary layer resistances of the canopy, R_n and
239 $R_{n(s)}$ are the net radiation above and below the canopy and r_a^s and r_a^a are the aerodynamic
240 resistances from soil to canopy and canopy to the reference height (= 2m) respectively, both
241 of which are estimated from wind speed and crop height following the approach described by
242 Shuttleworth and Gurney (1990) and Zhou et al. (2006). Assuming that only half the leaf area
243 contributes to transpiration, the canopy surface resistance r_s^c (s m^{-1}) can be expressed as:

$$244 \quad r_s^c = \frac{2}{\{k_{sto(max)} f_L f_{t(c)}\} LAI} \quad (8)$$

245 where $k_{sto(max)}$ is the maximum leaf stomatal conductance (m s^{-1}), LAI is the leaf area index (m^2
246 m^{-2}), $f_{t(c)}$ is a function describing the response of conductance to air temperature (see
247 *Environmental stress functions*) and f_L is a light response function given by:

$$248 \quad f_L = \left(\frac{R_i}{R_i + R_{50}} \right) \quad (9)$$

249 where R_i is the incoming radiation ($\text{MJ m}^{-2} \text{ d}^{-1}$) and R_{50} is the half-saturation constant for light
250 (here fixed at $5 \text{ MJ m}^{-2} \text{ d}^{-1}$). The bulk boundary layer resistance r_a^c (m s^{-1}) is given by:

$$251 \quad r_a^c = \frac{r_b}{LAI} \quad (10)$$

252 where r_b is the leaf boundary layer resistance (here fixed at 25 s m^{-1}). Radiation interception
253 by the plant canopy is calculated using Beer's law:

$$254 \quad R_{n(s)} = R_n (1 - f_{int}) \quad (11)$$

$$255 \quad f_{int} = 1 - e^{-\beta LAI} \quad (12)$$

256 where f_{int} is the fraction of the net radiation intercepted by the plant canopy and β is the
257 extinction coefficient. Net radiation is estimated from incoming solar radiation R_i using the
258 algorithms described in Allen et al. (1998).

259 Rainfall interception is at present not considered in the model. Although interception losses
260 may not be negligible even for a reasonably short grassland plant community (Ataroff and
261 Naranjo, 2009; Hu et al., 2009; Groh et al., 2019), we assume that the errors introduced by
262 ignoring the net increase in evaporation due to rainfall interception will be negligible.

263 2.2.2 Water flow, root water uptake and transpiration

264 Some SVAT models use tipping bucket or reservoir models to describe water storage and flow
265 in the soil, even though physical approaches based on Richard's equation are not difficult to
266 parameterize and usually perform better (e.g. Diekkrüger et al., 1995; Kröbel et al., 2010;
267 Guest et al., 2017). Water uptake by plant roots is also represented empirically in many widely
268 used SVAT models (Wang and Smith, 2004; Smithwick et al., 2014). These two issues are to
269 some extent linked, as physics-based models of root water uptake require information on soil
270 water pressures, while tipping bucket or reservoir models only simulate soil water contents.



271 In principle, water uptake by roots also depends on the 3D architecture of the plant root
 272 system as well as the hydraulic properties along multiple flow pathways in the soil and plant
 273 (e.g. Raats, 2007). Physics-based models have been developed that can calculate water flow
 274 and uptake by a root system explicitly defined in 3D (e.g. Dunbabin et al., 2013; Schnepf et al.,
 275 2018). Although some attempts have been made (e.g. Postma et al., 2017; Mboh et al., 2019),
 276 these models are not so well suited to coupling to SVAT models due to their high parameter
 277 and computational requirements. However, some parsimonious physics-based macroscopic
 278 approaches have been developed (e.g. de Jong van Lier et al., 2008, 2013; Couvreur et al.,
 279 2012; Javaux et al., 2013; Sulis et al., 2019) that contain no more parameters than the
 280 empirical models. The parameters of these models are also easier to estimate since they have
 281 a stronger physical basis (de Willigen et al., 2012; Javaux et al., 2013). For the same reason,
 282 the predictive use of these models should also be more robust in principle. The simplest
 283 physics-based models (e.g. Raats, 2007; de Jong van Lier et al., 2008) only describe flow to the
 284 roots and neglect flow and resistances within the plant. In this study, we use the model of root
 285 water uptake described by de Jong van Lier (2008), which is coupled with Richards' equation
 286 to calculate transient water flow soil water content, θ (m m^{-3}) in a one-dimensional soil profile:

$$287 \quad \frac{d\theta}{dt} = \frac{d}{dz} \left[K(\theta) \left(\frac{d(\psi+z)}{dz} \right) \right] - U \quad (13)$$

288 where t is time (days), z is height (m), K is the soil hydraulic conductivity (m day^{-1}), ψ is the
 289 pressure head (m) and U (days^{-1}) is the so-called sink term which accounts for root water
 290 uptake. The bottom boundary condition required to solve Richards' equation is specified as
 291 the known (measured) pressure head at the base of the simulated soil profile, i.e. at 1.4 m
 292 depth. The upper boundary condition to equation 13 is specified as a flux given by the
 293 difference between the known precipitation rate and the actual soil evaporation, E_a , which in
 294 turn is given by:

$$295 \quad E_a = \min(q_{max}; E_p) \quad (14)$$

296 where q_{max} is the maximum flow rate towards the soil surface calculated using Darcy's law
 297 from the pressure head in the uppermost soil layer. The soil water retention and hydraulic
 298 conductivity functions required to solve equation 13 are given by the Mualem-van Genuchten
 299 model (Mualem, 1976; van Genuchten, 1980), with the matching point hydraulic conductivity,
 300 K_{10} (m day^{-1}) set at a pressure head of -0.1 m (Luckner et al., 1989) and assuming that the
 301 residual water content is negligible:

$$302 \quad S = \frac{\theta}{\theta_s} \quad (15)$$

$$303 \quad S = (1 + |\alpha \psi|^n)^{\frac{1}{n}-1} \quad (16)$$

$$304 \quad K(S) = K_{10} \left(\frac{S}{S_{10}} \right)^\tau \left[\frac{1 - (1 - S(\frac{n}{n-1}))^{(1-\frac{1}{n})}}{1 - (1 - S_{10}(\frac{n}{n-1}))^{(1-\frac{1}{n})}} \right]^2 \quad (17)$$



305 where S is the degree of saturation (-), S_{10} is the value of S at a pressure head of -0.1 m, θ_s is
 306 the saturated water content ($\text{m}^3 \text{m}^{-3}$), α (m^{-1}) and n (-) are shape parameters and τ is a
 307 tortuosity/connectivity factor.

308 Neglecting water storage changes in the plants, the total water uptake from the root zone
 309 equals the actual transpiration rate, T_a , such that:

$$310 \quad T_a = \sum_i U_i \Delta z_i \quad (18)$$

311 where the subscript i refers to a layer in the root zone and Δz is its thickness. To calculate the
 312 sink term U_i and actual transpiration T_a , we make use of the parsimonious physics-based
 313 model of root water uptake proposed by de Jong van Lier et al. (2008), which implicitly
 314 accounts for compensatory uptake (Jarvis, 2011). Neglecting plant resistances, they derived
 315 the macroscopic water uptake sink term to Richards' equation by upscaling a model of water
 316 flow to a single root based on the concept of matric flux potential M ($\text{m}^2 \text{day}^{-1}$):

$$317 \quad M_i = \int_{\psi_w}^{\psi} K(\psi) d\psi \quad (19)$$

318 where ψ_w is the soil water pressure head at which water uptake by plants ceases. At the
 319 microscopic scale in the soil, M will continuously decrease towards its value at the root/soil
 320 interface M_o . In this study, we used the approximate solution derived by de Jong van Lier et
 321 al. (2009) to calculate M for the van Genuchten-Mualem model of soil hydraulic properties.
 322 Assuming that M_o is constant in the root zone and neglecting the effects of root and plant
 323 resistances on flow through the soil-plant system, de Jong van Lier et al. (2008) showed that
 324 the sink term for water uptake by roots in each soil layer can be expressed as:

$$325 \quad U_i = \rho_i (M_i - M_o) \quad (20)$$

326 where ρ is a composite root parameter (m^{-2}) given by (de Jong van Lier, 2008):

$$327 \quad \rho_i = \frac{4}{r_o^2 - a^2 r_{m(i)}^2 + 2(r_o^2 + r_{m(i)}^2) \text{LN}\left(\frac{a r_{m(i)}^2}{r_o^2}\right)} \quad (21)$$

328 where r_o is the root radius, a is the distance to the root (normalized by r_m) at which the soil
 329 water content is equal to the average value in layer i (fixed here at 0.53; de Jong van Lier et
 330 al., 2008) and r_m is the mean half distance to the root surface, which can be calculated from
 331 the effective root length density $R_{LD(i)}$ (m m^{-2}) as:

$$332 \quad r_{m(i)} = \sqrt{\frac{1}{\pi R_{LD(i)}}} \quad (22)$$

333 Actual transpiration is determined by the minimum of the potential transpiration rate, T_p , and
 334 the maximum possible flow rate of water to the root system, T_{max} , which occurs when $M_o=0$
 335 (see equations 18 and 20). Thus, actual transpiration can also be expressed as:

$$336 \quad T_a = \min(T_{max}; T_p) \quad (23)$$

337 where T_{max} is obtained by combining equations 18 and 20 with $M_o=0$:

$$338 \quad T_{max} = \sum_i \rho_i M_i \Delta z_i \quad (24)$$



339 For unstressed plants, $T_{max} \geq T_p$ and $T_a = T_p$. In this case, the unknown value of M_o in equation
340 20 is calculated by combining equations 18, 20 and 24 and knowing that $T_a = T_p$, which gives:

$$341 \quad M_0 = \frac{T_{max} - T_p}{(\sum_i \rho_i \Delta z_i)} \quad ; \quad T_{max} \geq T_p \quad (25)$$

$$342 \quad M_0 = 0 \quad ; \quad T_{max} < T_p$$

343 It can be seen from equations 24 and 25 that in any given soil, plant water stress will set in
344 earlier when potential transpiration rates are high and total root length density is low.

345 2.2.3 Growth model for perennial grassland

346 Even though detailed growth models designed for perennial forage grass are already available
347 (e.g. Schapendonk et al., 1998; Jing et al., 2012; Persson et al., 2014; Kellner et al., 2017), we
348 developed a simple generic model for the purpose of this study, which only simulates
349 vegetative growth. This model is intended to be able to capture the main longer-term
350 feedback mechanisms between soil water status and grass growth (Tardieu and Parent, 2017)
351 and is designed to be compatible with simpler water uptake models that do not simulate water
352 potentials, resistances and flows within plants (Manzoni et al., 2013).

353 In the model, net assimilation is calculated using the concept of radiation use efficiency (e.g.
354 Sinclair and Muchow, 1999), which implicitly assumes a constant ratio of respiration to
355 photosynthesis (i.e. carbon use efficiency; Gifford, 2003). Furthermore, we assume that
356 assimilation is limited by light, water and temperature, but not by sub-optimal nutrition. The
357 allocation of assimilates to above- and below-ground biomass depends on environmental
358 stressors. In this respect, based on empirical knowledge, we assume that water stress and sub-
359 optimal temperatures will increase the partitioning of assimilates to roots (e.g. Jones et al.,
360 1980a; Kahmen et al., 2005; Hui and Jackson, 2006; Wedderburn et al., 2010; Skinner and
361 Comas, 2010; Padilla et al., 2013; Nosalewicz et al., 2018; Meurer et al., 2019). Excess
362 carbohydrates produced by grasses during periods of “sink-limited” growth are stored as non-
363 structural reserves, mostly in the tiller bases and roots (Thomas, 1991; Johansson, 1993;
364 Volaire et al., 1998; Thomas and James, 1999; Østrem et al., 2011; Martínez-Vilalta et al., 2016;
365 Hofer et al., 2017; Katata et al., 2020). These non-structural carbohydrates contribute to rapid
366 recovery of growth after drought or defoliation by grazing or harvesting (Morvan-Bertrand et
367 al., 1999; Jing et al., 2012; Schmitt et al., 2013; Benot et al., 2019). However, for the sake of
368 simplicity, our growth model only tracks total biomasses in above- and below-ground
369 compartments and does not explicitly account for reserves of non-structural carbohydrates.

370 The loss of both above- and below-ground biomass by diverse mechanisms (e.g. herbivory,
371 exudation, root decay) is modelled in a simple way as a lumped first-order process. Although
372 root longevity can be affected by drought (e.g. Chen and Brassard, 2013), this is neglected in
373 the model for reasons of simplicity. Root systems also show plastic responses to
374 environmental conditions, such that growth of new roots takes place where water is easily
375 available, while root dieback occurs in dry soil (e.g. Jupp and Newman, 1987; DaCosta et al.,
376 2004; Wedderburn et al., 2010). Dynamic modeling of root proliferation and loss in response
377 to soil conditions remains a very difficult task (e.g. Wang and Smith, 2004; Boote et al., 2013;



378 Smithwick et al., 2014; Stöckle and Kemanian, 2020). Here, for the sake of simplicity, we
 379 assume that the distribution of root biomass and length within the root zone are constant, as
 380 well as the maximum depth of roots in the profile. With these assumptions, changes in the
 381 below-ground (root) biomass in any soil layer i , $B_{bg(i)}$ (kg dry matter m^{-2}) are given by:

$$382 \quad \frac{dB_{bg(i)}}{dt} = f_{bg} A f_{r(i)} - k_{bg} B_{bg(i)} \quad (26)$$

383 where k_{bg} is a first-order rate constant for root biomass loss (d^{-1}), A ($kg\ m^{-2}\ d^{-1}$) is the dry matter
 384 assimilation rate, f_{bg} is the fraction of dry matter production partitioned to roots and $f_{r(i)}$ is the
 385 fraction of this root production allocated to layer i , which is prescribed by a logistic dose
 386 response function (Schenk and Jackson, 2002; Fan et al., 2016; Metselaar et al., 2019):

$$387 \quad f_{r(i)} = \left[\frac{1}{1 + \left(\frac{D_U}{D_{50}}\right)^c} \right] - \left[\frac{1}{1 + \left(\frac{\min(D_L; D_r)}{D_{50}}\right)^c} \right] ; \quad D_r > D_U \quad (27)$$

$$388 \quad f_{r(i)} = 0 ; \quad D_r \leq D_U$$

389 where c is a shape factor, D_U and D_L are the depths to the upper and lower boundaries of layer
 390 i , D_r is an effective root depth, which we define as the depth above which 95% of the roots are
 391 located and D_{50} is the depth above which 50% of the root biomass is found, such that:

$$392 \quad D_{50} = \frac{D_r}{\left(\frac{1}{0.95} - 1\right)^{\frac{1}{c}}} \quad (28)$$

393 With this approach, 5% of the roots are located below the maximum root depth. In the model,
 394 we distribute this extra root biomass to the uppermost two numerical layers in equal amounts.

395 The assimilation rate A in equation 26 is calculated as a function of incoming solar radiation
 396 R_s ($MJ\ m^{-2}\ day^{-1}$) and two dimensionless stress functions, $f_{t(p)}$ and $f_{w(p)}$ varying between zero
 397 and unity to represent the effects of temperature and water stress on dry matter production:

$$398 \quad A = f_{int} R_s RUE_{max} f_{t(p)} f_{w(p)} \quad (29)$$

399 where RUE_{max} is the maximum radiation use efficiency ($kg\ MJ^{-1}$). The root allocation fraction
 400 f_{bg} in equation 26 is calculated as a function of plant stressors (i.e. air temperature, water
 401 stress) and “sink strength”, represented here by the fraction of radiation intercepted, f_{int} , using
 402 an approach based on the simple model concept outlined by Friedlingstein et al. (1999):

$$403 \quad f_{bg} = f_{bg(opt)} \left(\frac{2 f_{int}}{f_{int} + \min(f_{t(a)}; f_{w(a)})} \right) \quad (30)$$

404 where $f_{bg(opt)}$ is the fraction of assimilates partitioned below-ground when the conditions for
 405 above-ground production are optimal (i.e. full canopy, optimal temperature and no water
 406 stress) and $f_{t(a)}$ and $f_{w(a)}$ are response functions to account for the effects of sub-optimal
 407 conditions of temperature and water on allocation. With this approach, sub-optimal
 408 environmental conditions (extreme air temperatures, plant water stress) increase the
 409 proportion of assimilates partitioned to roots, whereas a loss of leaf area (e.g. due to harvest)
 410 triggers an increased allocation of assimilates to the above-ground biomass (see figure S5).



411 Changes in above-ground biomass, B_{ag} (kg m^{-2}) are given by:

$$412 \frac{dB_{ag}}{dt} = (1 - f_{bg})A - k_{ag} \max(1 - f_{t(a)}; 1 - f_{w(a)})B_{ag} - \Gamma \left(1 - \frac{H_{cut}}{H}\right) \left(\frac{B_{ag}}{\Delta t}\right) \quad (31)$$

413 where Γ is a binary variable, indicating the occurrence of harvest of above-ground biomass
414 (zero for no harvest, 1 for harvest), H_{cut} is the cutting height at harvest (here set to 0.01 m), H
415 is the grass height at harvest (m), Δt is the time step in the model and k_{ag} is a rate coefficient
416 (d^{-1}) regulating the loss of above-ground biomass by senescence and leaf fall, which is also
417 promoted by sub-optimal temperatures or plant water stress, employing the same empirical
418 functions used for assimilate partitioning between above-and below-ground biomass. In this
419 model, we do not account for standing dead above-ground biomass, which would alter the
420 partitioning of solar radiation between soil and plant, without contributing to transpiration
421 and assimilation, since we assume that the loss of green leaf area results in immediate litter-
422 fall. However, it would be straightforward to incorporate standing dead biomass in future
423 versions of the model, for example in the way described by Montaldo et al. (2005).

424 Feedbacks from the plant growth model to the hydrological model are provided by the leaf
425 area index, LAI, and effective root length density, $R_{LD(i)}$, which are calculated as:

$$426 LAI = B_{ag} S_{leaf} \quad (32)$$

$$427 R_{LD(i)} = \varepsilon \left(\frac{B_{bg(i)}}{z_i}\right) S_{root} \quad (33)$$

428 where S_{leaf} ($\text{m}^2 \text{kg}^{-1}$) and S_{root} (m kg^{-1}) are the specific leaf area and specific root length and ε is
429 the fraction of the total root length that is effective for water uptake (Faria et al., 2010). The
430 height of the crop also acts as a feedback control on the water balance, since it affects the
431 aerodynamic resistances to evapotranspiration (equations 1 to 7). The height of the grass
432 cover is not explicitly simulated in our relatively simple growth model. Instead, we calculate
433 plant height as a function of simulated LAI, based on the data from both sites (see figure S6).

434 2.2.4 Environmental stress functions

435 As in other models of crop growth (Wu et al., 2016), we use the ratio of actual to potential
436 transpiration to represent the effects of water stress on assimilation via stomatal closure:

$$437 f_{w(p)} = \frac{T_a}{T_p} \quad (34)$$

438 Water stress also limits crop growth without affecting photosynthesis by several different
439 mechanisms (Körner, 2015; White et al., 2016; Tardieu et al., 2018; Loka et al., 2019; Gupta et
440 al., 2020). Many crop models calculate limitations on leaf growth as a threshold function of
441 the soil water deficit in the root zone. Here, we make use of the matric flux potential at the
442 root surface M_o (see equations 20 and 25) as a measure of plant water stress, since it should
443 be more physically and physiologically meaningful. We therefore define a second water stress
444 index as a threshold response function of M_o , varying between zero and unity, which regulates
445 dry matter allocation and leaf loss in the model (equations 30 and 31):



$$446 \quad f_{w(a)} = 1 \quad ; \quad M_o \geq M_{o(crit)} \quad (35)$$

$$447 \quad f_{w(a)} = \frac{M_o}{M_{o(crit)}} \quad ; \quad M_o < M_{o(crit)}$$

448 where $M_{o(crit)}$ is a critical value of M_o , which is in turn calculated from a user-defined value of
449 a critical pressure head at the soil/root interface, $\psi_{o(crit)}$.

450 As in many soil-crop models (Wu et al., 2016), the temperature response function in equations
451 8 and 29 to 31 is modelled with a piece-wise linear function (figure S7):

$$452 \quad f_{t(c,p,a)} = 0 \quad ; \quad T < T_b \text{ or } T > T_c \quad (36)$$

$$453 \quad f_{t(c,p,a)} = \left(\frac{T - T_b}{T_{o(low)} - T_b} \right) \quad ; \quad T_b \leq T \leq T_{o(low)}$$

$$454 \quad f_{t(c,p,a)} = \left(\frac{T_c - T}{T_c - T_{o(high)}} \right) \quad ; \quad T_{o(high)} \leq T \leq T_c$$

$$455 \quad f_{t(c,p,a)} = 1 \quad ; \quad T \geq T_{o(low)} \text{ and } T \leq T_{o(high)}$$

456 where T is the mean air temperature ($^{\circ}\text{C}$), $T_{o(low)}$ and $T_{o(high)}$ define the optimum temperature
457 ($^{\circ}\text{C}$) range at which $f_{t(p,a)}$ equals unity and T_b and T_c are the base and ceiling temperatures ($^{\circ}\text{C}$)
458 at which the function equals zero. Different values for the parameters in equation 36 can be
459 assigned for transpiration ($f_{t(c)}$), assimilation ($f_{t(p)}$) and allocation and leaf fall ($f_{t(a)}$).

460 2.3 Model application

461 2.3.1 Modelling strategy

462 In this study, uncertainty in the model parameterization has been addressed through Monte
463 Carlo simulations following the GLUE methodology (see *Sensitivity and uncertainty analysis*).
464 In principle, it would be possible to apply the model individually to each lysimeter in such an
465 approach. However, this would have been far too demanding of computer resources. Instead,
466 recognizing the comparatively small differences in hydrological behavior among the three
467 replicates at each site (Table 1) and the fact that the same soil type is present at both sites,
468 we decided to simplify the analysis by assuming a common parameterization for the soil
469 hydraulic properties in all six lysimeters. Similarly, we also neglected the small differences in
470 boundary conditions among the replicate lysimeters at each site. Thus, precipitation (Table 1;
471 figure S1) and pressure heads at the bottom boundary (figure S4) measured for one lysimeter
472 at each site (Ro_Y_015 at Rollesbroich and Se_Y_026 at Selhausen) were used to represent all
473 three replicates. This approach also implicitly assumes that we can neglect the likelihood of
474 small differences in initial conditions among the replicates at each site. Initial soil water
475 pressure head profiles at each site were set according to the results of preliminary simulations
476 involving “trial and error” calibration to measured early time water outflows from the
477 lysimeters. Initial above- and below-ground plant biomasses were calculated assuming that
478 the roots constituted 80% of the total biomass and that the initial leaf area index was 1.5. It
479 can be noted that model predictions quickly become independent of these initial guesses.



480 2.3.2 Soil hydraulic parameters

481 Four horizons were identified from a soil profile description at the Rollesbroich site (Table 1).
482 Common parameters of the Mualem-van Genuchten model were estimated for each horizon
483 from a combination of direct measurements and pedotransfer functions (Table 3). The paired
484 TDR and tensiometer measurements obtained in the lysimeters at 30 and 50 cm depth were
485 utilized to estimate common water retention parameters at the two sites for the horizons at
486 24-48 and 48-90 cm depth by least-squares fitting (Table 3 and figure S3). We used the HYPRES
487 class pedotransfer functions (Wösten et al., 1999) to estimate the van Genuchten water
488 retention parameters from the soil textural class in the deep subsoil (90-140 cm depth) where
489 no data was available. The measurements from the matric potential sensors installed in the
490 uppermost soil horizon (0-24 cm depth) appeared to be unreliable. We therefore also used
491 the HYPRES pedotransfer functions to estimate the shape parameter n in the topsoil, while α
492 was set equal to the same value as the deeper horizons. Saturated water contents clearly
493 differed between the two sites in the uppermost horizon and were estimated from the data
494 by eye. Hydraulic conductivity at a pressure head of -10 cm (see table 3) was estimated from
495 clay content in each horizon using the pedotransfer function developed by Jarvis et al. (2013).

496 2.3.3 Sensitivity and uncertainty analysis

497 A comprehensive uncertainty analysis treating a large number of model parameters as
498 uncertain was not feasible in this study from the point of view of both data support and
499 computational capacity, even for the comparatively parsimonious model used in this study.
500 We therefore performed a preliminary Monte Carlo sensitivity analysis to support the
501 selection of a limited number of parameters to include in the uncertainty analysis. We ran 500
502 simulations for each site for the period 2013-2018 with parameter values obtained by Latin
503 hypercube sampling from uniform distributions (table S2 in the supplementary information).
504 We quantified the sensitivity of two target outputs (i.e. total evapotranspiration and harvest
505 during the experimental period) to model parameters using Spearman rank partial correlation
506 coefficients. The sampled ranges for the plant parameters in the model were selected to
507 reflect variations based on information in the literature. Three soil hydraulic parameters were
508 also included in this analysis (K_{10} , α and n). This was done by applying scaling factors (see table
509 S2) to the parameter values in Table 3 to broadly reflect the uncertainty arising from the use
510 of pedotransfer functions as well as the spatial variations in the water retention curves derived
511 from the lysimeter measurements (figure S3). It should be noted here that the resulting ranges
512 adopted for the two van Genuchten parameters encompass the differences found among the
513 six lysimeters at both depths. Table S2 shows the results. In general, evapotranspiration and
514 harvest is much more sensitive to many of the plant parameters than to variation in the soil
515 hydraulic properties, which lends support to a modelling strategy in which soil hydraulic
516 properties are set to identical values for all lysimeters. We therefore focused the uncertainty
517 analysis on investigating differences in key plant parameters between the two sites.

518 Of the many highly sensitive plant parameters (Table S2), we decided to treat four as
519 uncertain: the radiation extinction coefficient β , the maximum stomatal conductance $k_{sto(max)}$,
520 the maximum root depth D_r and the limiting pressure head $\psi_{0(crit)}$ that controls dry matter
521 (DM) allocation between above- and below-ground compartments as well as the rate of leaf



522 loss. Several subjective criteria underpin this selection. Firstly, they are among the most highly
523 sensitive parameters for both evapotranspiration and harvest yields (Table S2). In this respect,
524 with the exception of $T_{o(low)}$, it seems that plant parameters controlling temperature response
525 are much less sensitive than those regulating water stress (Table S2). Secondly, in addition to
526 the changes in plant community composition, there are also some known mechanisms of plant
527 acclimation (e.g. Vincent et al., 2020) that could explain why these four parameters might
528 plausibly take different values at the two sites. Finally, the effects on these four model
529 parameters on the model outputs are unlikely to be strongly correlated with one another. This
530 would not be the case for some of the other sensitive parameters. For example, the radiation
531 extinction coefficient β would be correlated with the maximum radiation use efficiency, while
532 $\psi_{o(crit)}$ would be correlated with both the parameter controlling DM allocation under optimal
533 conditions, $f_{bg(opt)}$, as well as the effective root fraction, ε . The remaining plant parameters in
534 the model were therefore set to fixed values estimated from data in the literature (Table 4),
535 prioritizing field studies rather than pot experiments, as the development of drought and the
536 plant response to stress are known to be strongly affected by restricted root zones (Jones et
537 al., 1980a,b). Specific leaf area was set to $142 \text{ cm}^2 \text{ g}^{-1}$ based on the measurements of above-
538 ground biomass and leaf area index for the combined dataset at both sites (see figure S6). The
539 relationship shown in figure S6 shows some scatter, but no systematic difference between the
540 sites is apparent. In this respect, Norris (1982) also found no significant differences in specific
541 leaf area for *Lolium perenne* in droughted, control and irrigated plots.

542 We used the GLUE (Generalized Likelihood Uncertainty Estimation; Beven and Binley, 1992;
543 Beven 2006) methodology to account for parameter uncertainty. The objective of this
544 informal Bayesian approach is not to find a single optimum parameter set by calibration, as it
545 acknowledges that many different parameterizations will perform equally well (so-called
546 “equifinality”), not least as a consequence of the inevitability of model (structural) error. The
547 objective of GLUE is therefore to identify acceptable (“behavioural”) parameterizations. To
548 support this analysis, we ran 2000 simulations for each site, with parameter sets determined
549 using Latin Hypercube sampling from the prior uncertainty ranges for the four uncertain
550 parameters shown in Table 5. GLUE involves several subjective decisions, two of the most
551 important ones being the choice of a likelihood function (i.e. a measure of goodness-of-fit)
552 and deciding on the criteria that should be used to determine whether a simulation is
553 acceptable or not. We considered that a parameterization was acceptable if two criteria were
554 satisfied. The first uses calculations of the model efficiency, ME , for the six observed time
555 series of data (i.e. water contents at three depths, evapotranspiration rates, LAI, harvests):

$$556 \quad ME = \frac{\sum_{i=1}^m (O_i - \bar{O})^2 - \sum_{i=1}^m (O_i - P_i)^2}{\sum_{i=1}^m (O_i - \bar{O})^2} \quad (37)$$

557 where O and P are the observed and simulated values for a given data type and m is the
558 number of observations. The maximum value of ME is one, when predictions and observations
559 are identical, while a negative value implies a poor model, since it means that taking the
560 average of the observations would give a better prediction. A simulation was considered
561 acceptable if i.) the model efficiency for all six data types was within 0.5 of the maximum value
562 for that data series, and ii.) both the simulated annual average evapotranspiration AET



563 (mm/year) and overall (apparent) water use efficiency WUE (kg DM m^{-3}) were within
564 acceptable limits roughly defined by the observations (see Table 2):

565 *At Rollesbroich: $610 < AET < 660$ and $1.0 < WUE < 1.2$*

566 *At Selhausen: $680 < AET < 730$ and $0.85 < WUE < 1.05$*

567 This second criterion ensures that the acceptable parameterizations respect the overall broad
568 differences observed in the water balance components and harvest yields between the two
569 sites. Note that the acceptable limit for WUE at Rollesbroich makes no attempt to “honour”
570 the data from lysimeter Ro_Y_013, since it is considered an outlier, as discussed earlier. In
571 total, 35 simulations at Rollesbroich and 57 at Selhausen satisfied these criteria. It is desirable
572 to have the same number of acceptable parameter sets at each site. From these acceptable
573 simulations, we therefore selected the 30 best simulations at each site (i.e. 1.5% of the total
574 number of simulations) according to the average model efficiency for the six data types.

575 3. Results and discussion

576 3.1 Acceptable parameter values

577 The distributions of the acceptable values for the four uncertain parameters are shown in
578 figure 3, while posterior parameter ranges defined by different percentiles of these
579 distributions are presented in table 5. The posterior uncertainty ranges are much smaller than
580 the prior uncertainty ranges, which suggests that values for all four uncertain parameters
581 were clearly identifiable from the data. No differences between the two sites were found for
582 two of the parameters, the radiation extinction coefficient β and $\psi_{o(crit)}$ the parameter
583 controlling dry matter allocation and leaf loss as a function of water stress ($p = 0.98$ and 0.16
584 respectively). The derived values of $\psi_{o(crit)}$ (median value of -271 cm at both sites, Table 5) are
585 much larger than ψ_w ($= -150$ m, Table 4), which indicates that water stress affects above-
586 ground plant growth long before stomatal closure limits transpiration and assimilation
587 (Staniak and Kocoń 2015; Körner, 2015; Loka et al., 2019). This has been shown experimentally
588 for droughted field-grown grass/clover pastures by Jones et al. (1980a,b) and Hofer et al.
589 (2017). The values of the radiation extinction coefficient (inter-quartile range = 0.51 - 0.65 at
590 both sites) are typical of values reported for grassland ecosystems (Zhang et al., 2014).

591 In contrast, the results of the GLUE analysis suggest that both the maximum root depth and
592 the unstressed stomatal conductance have increased significantly for the lysimeters moved to
593 Selhausen ($p < 0.0001$ for both). The estimated root depth at Rollesbroich (ca. 56 cm) matches
594 observations made at the site at the time of extraction of the lysimeters reasonably well. The
595 simulations suggest that the maximum root depth at Selhausen has increased to ca. 80 cm,
596 while the maximum stomatal conductance has roughly doubled. The mechanisms underlying
597 these changes are not clear. One reason may be the significant changes observed in the plant
598 community composition at Selhausen compared with the original resident plant community
599 (figure S2), as plant traits may differ significantly between herbs and grasses. Another likely
600 reason is that one or more of the dominant species adapted to the new climate. In this respect,
601 plants are known to acclimatize to environmental stresses at a range of time-scales by various
602 physiological and morphological mechanisms (e.g. Maseda and Fernández, 2006; Nicotra et



603 al., 2010; Nicotra and Davidson, 2010; Manzoni et al., 2013; Bartlett et al., 2014; Tardieu et
604 al., 2018; Vincent et al., 2020).

605 **3.2 Soil hydrology**

606 Figures 4 and 5 show comparisons of the acceptable simulations at the two sites with the soil
607 water contents measured at the three depths in the lysimeters and daily evapotranspiration
608 rates respectively. The model efficiencies for these simulations are shown in table 6. Figure 6
609 compares measured annual average evapotranspiration and percolation in the period 2013-
610 2018 with the simulations. Taken together, these results show that the model performs very
611 well, matching the temporal dynamics in the high-time resolution data on state variables and
612 fluxes as well as reproducing the differences in the overall water balances at the two sites.
613 This is probably because the macroscopic sink term describing root water uptake that we
614 coupled to Richards' equation has a reasonably strong physical basis. In particular, this model
615 implicitly accounts for the mechanism of "compensatory" root water uptake, something which
616 is clearly necessary in order to reproduce the extensive drying in the root zone observed in
617 the Selhausen lysimeters, with very little reduction in water uptake and transpiration.

618 Figure 7 shows some terms of the simulated water balances that were not measured. Potential
619 evapotranspiration calculated internally in the model by the Shuttleworth-Wallace version of
620 the Penman-Monteith equation as a dynamic function of leaf area development at the two
621 sites is very similar to the estimates obtained by the FAO version (Figure 7; table 2), which
622 only treats the vegetation implicitly. This is in spite of the fact that the balance between
623 simulated soil evaporation and transpiration differs strongly between the two sites, with soil
624 evaporation being a much larger component of the water balance at Rollesbroich (Figure 7),
625 where it comprises ca. 70% of the total evapotranspiration. There may be several reasons why
626 soil evaporation is such an important term in the water balance at Rollesbroich, including the
627 wet climate with high wind speeds (Groh et al., 2019) the capillary nature of the soil and also
628 the fact that the grassland is harvested 3-4 times during the growing season, which exposes
629 the soil surface to evaporation. In contrast, soil evaporation is much smaller (ca. 50% of total
630 evapotranspiration) in the drier climate at Selhausen, presumably because drying of the soil
631 surface in summer frequently reduced evaporation below the potential rate (figure 7).

632 Figure 7 shows that the model simulates only small reductions of transpiration due to water
633 stress and stomatal closure at both sites ($T_a < T_p$), which matches the inference derived from
634 comparing the lysimeter data with the FAO estimates of potential evaporation (figure 1). This
635 result is not especially surprising for the grassland growing in the wet climate at Rollesbroich,
636 but it does require further analysis and explanation for the much drier Selhausen site. Figure
637 8 shows the simulated time-courses of the two water stress functions in the model. Short
638 periods of stomatal closure induced by water stress occur every summer at Selhausen in most
639 of the acceptable model simulations, with one more extended period of drought stress (ca. 1
640 to 2 weeks) in 2018. However, overall, the extent and severity of reductions in transpiration
641 due to water stress simulated at Selhausen is not much larger than at Rollesbroich. The reason
642 for this becomes apparent from a comparison of the results for the two highlighted
643 simulations in figure 8. This comparison illustrates the fact that simulations with strong
644 reductions in the dry matter allocation function show correspondingly small reductions in the



645 stress function regulating transpiration or, as in this example (simulation number 6), none at
646 all. This is because an increased rate of leaf loss and a greater allocation of assimilates to the
647 below-ground biomass during drought reduces the transpiration demand as well as increasing
648 the potential rate of water uptake by the root system. These adaptation mechanisms in
649 response to soil drying conserve soil water and reduce the likelihood of stomatal closure, so
650 that transpiration can be maintained during extended dry summer periods at Selhausen.

651 **3.3 Grassland growth**

652 Figures 9 and 10 show comparisons of the acceptable simulations with the measurements of
653 leaf area index and harvested biomass on the lysimeters at Selhausen and Rollesbroich. The
654 model efficiencies for these two data types are shown in table 6. Figure 11 shows box and
655 whisker plots of the simulated total harvest and overall water use efficiencies (WUE, defined
656 as total harvest divided by evapotranspiration) at the two sites. The results suggest that the
657 model performed satisfactorily for leaf area development at both sites and for harvested
658 biomass at Selhausen, but not for harvests at Rollesbroich (table 6). These poorer results can
659 largely be explained by the fact that lysimeter Ro_Y_013 was considered an outlier, so no
660 effort was made to match this data by loosening the constraints in the GLUE analysis.

661 Figure 12 shows the gain and loss terms in the dry matter balances simulated with the 30 best
662 parameterizations at each site. Simulated assimilation was ca. 10% larger at Selhausen
663 compared with Rollesbroich as a consequence of the greater radiation input and higher
664 temperatures (Figure S1) and the fact that water stress is only slightly more prevalent (Figure
665 8). Leaf loss is a relatively small term in the mass balance (10-12% of assimilation) and is similar
666 at both sites (Figure 12). Root production and decay (i.e. turnover) are more significant terms,
667 with root decay closely mirroring production, since it is modelled as a first-order function of
668 biomass. Expressed as a proportion of assimilation, simulated root production and decay is
669 somewhat larger at Selhausen compared with Rollesbroich (ca. 58 and 53% of assimilation
670 respectively, on average, for both), while root biomass is also somewhat larger at Selhausen
671 (see figure S8). This is in agreement with experimental studies that have demonstrated
672 increases in below-ground biomass production in grasslands as a consequence of drought (e.g.
673 Jones et al., 1980a; Kahmen et al., 2005; Wedderburn et al., 2010; Skinner and Comas, 2010;
674 Padilla et al., 2013; Nosalewicz et al., 2018; Meurer et al., 2019). It was not possible to make
675 measurements of root biomass and production in the lysimeters at the two sites due to the
676 constraints of the experimental set-up. However, literature data on root biomass and
677 production in similar temperate grassland environments can serve as an approximate “reality-
678 check”, suggesting that our simulations (Figure S8) are reasonable. For example, in northern
679 Germany, Chen et al. (2016) measured a root biomass of ca. 500 g m⁻² at 0-30 cm depth and a
680 growth rate of 450 g m⁻² year⁻¹, while in central Sweden, Meurer et al. (2019) found a root
681 biomass of 250-330 g m⁻² in the same depth interval. In central France, Picon-Cochard et al.
682 (2012) reported summer peak root biomasses of 13 perennial grasses grown in monoculture
683 varying between ca. 400 and 800 g m⁻², with a temporal pattern matching that simulated by
684 our model (Figure S8). Likewise, Wedderburn et al. (2010) reported peak root counts in early
685 summer and a minimum in winter for *Lolium perenne* pastures in New Zealand. The values of



686 below-ground production simulated by our model are also within the range reported by Hui
687 and Jackson (2006) for temperate grasslands in a global meta-analysis.

688 **4. Conclusions**

689 In this study, we made use of an eco-hydrological model to analyze the impacts on soil water
690 balance and grassland production of climate change triggered by the transfer of weighing
691 lysimeters from a wet, cool climate (Rollebroich) to a drier, warmer climate (Selhausen). The
692 relatively simple model employed in this study gave excellent simulations of soil water
693 contents (Model Efficiency, ME, between 0.24 and 0.87) and evapotranspiration rates (ME
694 between 0.32 and 0.60) measured at a daily resolution at both sites during a six-year period,
695 as well as acceptable simulations of leaf area development (ME between -0.04 and 0.50). In
696 this model application, we assumed identical static root distributions for the grassland at the
697 two sites and inferred different (constant) values of the maximum root depth, with deeper
698 roots in the drier climate at Selhausen. We also concluded from the modelling that more
699 frequent and intense soil drying at Selhausen led to a shift towards a greater production of
700 below-ground biomass. A major challenge for the future will be to further develop crop and
701 eco-hydrological models to enable them to predict these dynamic responses of plant roots to
702 changing soil and climatic conditions as emergent phenomena. In this respect, it should be
703 worthwhile to test simple empirical approaches to link root distribution with maximum root
704 depth and biomass (e.g. Arora and Boer, 2003) as well as developing improved architectural
705 models of root growth (e.g. Postma et al., 2017; Schnepf et al., 2018; Mboh et al., 2019).
706 Regardless of modelling approach, it seems clear that plastic responses of plant traits to
707 climate change of the kind we inferred from our study (e.g. in root depth or leaf conductance)
708 introduce significant uncertainties into model predictions of water balance and plant growth.

709 **Data availability**

710 The raw data can be freely obtained from the TERENO data portal (<https://teodoor.icg.kfa-juelich.de/ddp/index.jsp>). Processed data developed during this study can be acquired upon
711 request from Jannis Groh or Katharina Meurer.
712

713 **Author contributions**

714 The study was conceived by NJ, HV, KM and EL. NJ built the model. TP, JG, WD and CB supplied
715 data and advised on its use. Initial data analyses and model applications were carried out by
716 ER as part of his thesis project, supervised by KM, NJ and EL. NJ and KM carried out the final
717 simulations. NJ prepared the manuscript with contributions from all authors.

718 **Competing interests**

719 The authors declare that they have no conflict of interest.

720 **Acknowledgments**

721 This work was partly funded by the Swedish Research Council for Sustainable Development
722 (FORMAS, grant no. 2018-02319). We also acknowledge the support of the TERENO-SoilCan
723 program funded by the Helmholtz Association (HGF) and the Federal Ministry of Education
724 and Research (BMBF). We would also like to thank Werner Küpper, Ferdinand Engels, Philipp



725 Meulendick, Rainer Harms, and Leander Fürst at the Selhausen and Rollesbroich lysimeter
726 stations for their support.



References

- Akmal, M., Janssens, M. 2004. Productivity and light use efficiency of perennial ryegrass with contrasting water and nitrogen supplies. *Field Crops Research*, 88, 143-155.
- Allen, R., Pereira, L., Raes, D., Smith, M. 1998. Crop evapotranspiration – guidelines for computing crop water requirements. FAO Irrigation and Drainage Paper 56, FAO Food and Agricultural Organization of the United Nations, Rome.
- Arora, V., Boer, G. 2003. A representation of variable root distribution in dynamic vegetation models. *Earth Interactions*, 7, Paper no.6, 1-19.
- Ataroff, M., Naranjo, M. 2009. Interception of water by pastures of *Pennisetum clandestinum* Hochst. ex Chiov. and *Melinis minutiflora* Beauv. *Agricultural and Forest Meteorology*, 149, 1616-1620.
- Bartlett, M., Zhang, Y., Kreidler, N., Sun, S., Ardy, R., Cao, K., Sack, L. 2014. Global analysis of plasticity in turgor loss point, a key drought tolerance trait. *Ecology Letters*, 17, 1580-1590.
- Beier, C., Beierkuhnlein, C., Wohlgemuth, T., Penuelas, J., Emmett, B., Körner, C., de Boeck, H., Hesselbjerg Christensen, J., Leuzinger, S., Janssens, I., Hansen, K. 2012. Precipitation manipulation experiments – challenges and recommendations for the future. *Ecology Letters*, 15, 899-911.
- Bellocchi, G., Rivington, M., Donatelli, M., Matthews, K. 2010. Validation of biophysical models: issues and methodologies. A review. *Agronomy for Sustainable Development*, 30, 109-130.
- Benot, M-L., Morvan-Bertrand, A., Mony, C., Huet, J., Sulmon, C., Decau, M-L., Prud'homme M-P., Bonis, A. 2019. Grazing intensity modulates carbohydrate storage pattern in five grass species from temperate grasslands. *Acta Oecologia*, 95, 108-115.
- Beven, K., Binley, A. 1992. The future of distributed models: model calibration and uncertainty prediction. *Hydrological Processes*, 6, 279-298.
- Beven, K. 2006. A manifesto for the equifinality thesis. *Journal of Hydrology*, 320, 18-36.
- Black, A., Moot, D., Lucas, R. 2006. Development and growth characteristics of Caucasian and white clover seedlings, compared with perennial ryegrass. *Grass and Forage Science*, 61, 442-453.
- Bogena, H., Montzka, C., Huisman, J., Graf, A., Schmidt, M., Stockinger, M., von Hebel, C., Hendricks-Franssen, H., van der Kruk, J., Tappe, W., Lücke, A., Baatz, R., Bol, R., Groh, J., Pütz, T., Jakobi, J., Kunkel, R., Sorg, J., Vereecken, H. 2018. The TERENO-Rur hydrological observatory: a multiscale multi-compartment research platform for the advancement of hydrological science. *Vadose Zone Journal*, 17:180055. doi:10.2136/vzj2018.03.0055
- Bollig, C., Feller, U. 2014. Impacts of drought stress on water relations and carbon assimilation in grassland species at different altitudes. *Agriculture, Ecosystems and Environment*, 188, 212-220.
- Bonos, S., Murphy, J. 1999. Growth responses and performance of Kentucky Bluegrass under summer stress. *Crop Science*, 39, 770-774.
- Boote, K., Jones, J., White, J., Asseng, S., Lizaso, J. 2013. Putting mechanisms into crop production models. *Plant, Cell and Environment*, 36, 1658-1672.
- Bossio, D., Cook-Patton, S., Ellis, P., Fargione, J., Sanderman, J., Smith, P., Wood, S., Zomer, R., von Unger, M., Emmer, I., Griscom, B. 2020. The role of soil carbon in natural climate solutions. *Nature Sustainability* doi.org/10.1038/s41893-020-0491-z, 391-398.



- Cai, G., Vanderborght, J., Couvreur, V., Mboh, C., Vereecken, H. 2017. Parameterization of root water uptake models considering dynamic root distributions and water uptake compensation. *Vadose Zone Journal*, 17:160125. doi:10.2136/vzj2016.12.0125.
- Chen, H., Brassard, B. 2013. Intrinsic and extrinsic controls of fine root life span. *Critical Reviews in Plant Sciences*, 32, 151-161.
- Chen, S., Lin, S., Reinsch, T., Loges, R., Hasler, M., Taube, F. 2016 Comparison of ingrowth core and sequential soil core methods for estimating belowground net primary production in grass-clover swards. *Grass and Forage Science*, 71, 515-528.
- Coleman, S., Shiel, R., Evans, D. 1989. The effects of weather and nutrition on the yield of hay from Palace Leas meadow hay plots, at Cockle Park experimental farm, over the period from 1897 to 1980. *Grass and Forage Science*, 42, 353-358
- Couvreur, V., Vanderborght, J., Javaux, M. 2012. A simple three-dimensional macroscopic root water uptake model based on the hydraulic architecture approach. *Hydrology and Earth System Sciences*, 16, 2957-2971.
- DaCosta, M., Wang, Z., Huang, B. 2004. Physiological adaptation of Kentucky Bluegrass to localized soil drying. *Crop Science*, 44, 1307-1314.
- de Jong van Lier, Q., van Dam, J., Metselaar, K., de Jong, R., Duijnisveld, W. 2008. Macroscopic root water uptake distribution using a matric flux potential approach. *Vadose Zone Journal*, 7, 1065-1078.
- de Jong van Lier, Q., Dourado Neto, D., Metselaar, K. 2009. Modeling of transpiration reduction in van Genuchten–Mualem type soils. *Water Resources Research*, 45, W02422, doi:10.1029/2008WR006938
- de Jong van Lier, Q., van Dam, J., Durigon, A., dos Santos, M., Metselaar, K. 2013. Modeling water potentials and flows in the soil-plant system comparing hydraulic resistances and transpiration reduction functions. *Vadose Zone Journal*, 12, doi: 10.2136/vzj2013.02.0039.
- de Willigen, P., van Dam, J., Javaux, M., Heinen, M. 2012. Root water uptake as simulated by three soil water flow models. *Vadose Zone Journal*, doi:10.2136/vzj2012.0018.
- Diekkrüger, B., Söndgerath, D., Kersebaum, K., McVoy, C. 1995. Validity of agroecosystem models a comparison of results of different models applied to the same data set. *Ecol. Model.*, 81, 3–29.
- Dunbabin, V., Postma, J., Schnepf, A., Pagès, L., Javaux, M., Wu, L., Leitner, D., Chen, Y., Rengel, Z., Diggel, A. 2013. Modelling root-soil interactions using three-dimensional models of root growth, architecture and function. *Plant Soil*, 372, 93-124.
- Eckersten, H., Herrmann, A., Kornher, A., Halling, M., Sindhøj, E., Lewan, E. 2012. Predicting silage maize yield and quality in Sweden as influenced by climate change and variability. *Acta Agriculturae Scandinavica, Section B – Soil and Plant Science*, 62, 151-165.
- Fan, J., McConkey, B., Wang, H., Janzen, H. 2016. Root distribution by depth for temperate agricultural crops. *Field Crops Research*, 189, 68-74.
- Faria, L., da Rocha, M., de Jong van Lier, Q., Casaroli, D. 2010. A split-pot experiment with sorghum to test a root water uptake partitioning model. *Plant Soil*, 331, 299-311.
- Fatichi, S., Pappas, C., Ivanov, V. 2016. Modeling plant-water interactions: an ecohydrological overview from the cell to the global scale. *WIREs Water* 3, 327-368. doi: 10.1002/wat2.1125



- Foley, J., Ramankutty, N., Brauman, K., Cassidy, E., Gerber, J., Johnston, M., Mueller, N., O'Connell, C., Ray, D., West, P., Balzer, C., Bennett, E., Carpenter, S., Hill, J., Monfreda, C., Polasky, S., Rockström, J., Sheehan, J., Siebert, S., Tilman, D., Zaks, D. 2011. Solutions for a cultivated planet. *Nature* 7369, 337-342.
- Forstner, V., Groh, J., Vremec, M., Herndl, M., Vereecken, H., Gerke, H., Birk, S., Pütz, T. 2021. Response of water balance components to climate change in permanent grassland soil ecosystems. *Hydrology and Earth System Sciences Discussions*. doi.org/10.5194/hess-2021-100.
- Friedlingstein, P., Joel, G., Field, C., Fung, I. 1999. Toward an allocation scheme for global terrestrial carbon models. *Global Change Biology*, 5, 755-770.
- Gebler, S., Hendricks Franssen, H-J., Pütz, T., Post, H., Schmidt, M., Vereecken, H. 2015. Actual evapotranspiration and precipitation measured by lysimeters: a comparison with eddy covariance and tipping bucket. *Hydrology and Earth System Sciences*, 19, 2145-2161.
- Gifford, R. 2003. Plant respiration in productivity models: conceptualisation, representation and issues for global terrestrial carbon-cycle research. *Functional Plant Biology*, 30, 171-186.
- Giraud, M., Groh, J., Gerke, H. H., Brüggemann, N., Vereecken, H., Pütz, T. 2021. Soil Nitrogen Dynamics in a Managed Temperate Grassland Under Changed Climatic Conditions. *Water*, 13, 931, doi.org/10.3390/w13070931
- Groh, J., Pütz, T., Gerke, H., Vanderborght, J., Vereecken, H. 2019. Quantification and prediction of nighttime evapotranspiration for two distinct grassland ecosystems. *Water Resources Research*, 55, 2961-2975.
- Groh, J., Diamantopoulos, E., Duan, X., Ewert, F., Herbst, M., Holbak, M., Kamali, B., Kersebaum, K.-C., Kuhnert, M., Lischeid, G., Nendel, C., Priesack, E., Steidl, J., Sommer, M., Pütz, T., Vereecken, H., Wallor, E., Weber, T., Wegehenkel, M., Weihermüller, L., Gerke, H. 2020a. Crop growth and soil water fluxes at erosion-affected arable sites: using weighing lysimeter data for model intercomparison. *Vadose Zone Journal* 19: e20058. doi:10.1002/vzj2.20058.
- Groh, J., Vanderborght, J., Pütz, T., Vogel, H-J., Gründling, R., Rupp, H., Rahmati, M., Sommer, M., Vereecken, H., Gerke, H. 2020b. Responses of soil water storage and crop water use efficiency to changing climatic conditions: a lysimeter-based space-for-time approach. *Hydrology and Earth System Sciences*, 24, 1211-1225.
- Guest, G., Kröbel, R., Grant, B., Smith, W., Sansoulet, J., Pattey, E., Desjardins, R., Jégo, G., Tremblay, N., Tremblay, G. 2017. Model comparison of soil processes in eastern Canada using DayCent, DNDC and STICS. *Nutrient Cycling in Agroecosystems*, 109, 211-232.
- Gupta, A., Rico Medina, A., Caño Delgado, A. 2020. The physiology of plant responses to drought. *Science*, 266-269.
- He, D, Wang, E., Wang, J., Robertson, M. 2017. Data requirement for effective calibration of process-based crop models. *Agricultural and Forest Meteorology*, 234-235, 136-148.
- Heinlein, F., Biernath, C., Klein, C., Thieme, C., Priesack, E. 2017. Evaluation of simulated transpiration from maize plants on lysimeters. *Vadose Zone Journal*, doi:10.2136/vzj2016.05.0042
- Hennessy, D., O'Donovan, M., French, P., Laidlaw, A. 2008. Factors influencing tissue turnover during winter in perennial ryegrass-dominated swards. *Grass and Forage Science*, 63, 202–211.



- Hofer, D., Suter, M., Buchmann, N., Lüscher, A. 2017. Severe water deficit restricts biomass production of *Lolium perenne* L. and *Trifolium repens* L. and causes foliar nitrogen but not carbohydrate limitation. *Plant Soil*, 421, 367-380.
- Hoover, D., Wilcox, K., Young, K. 2018. Experimental droughts with rainout shelters: a methodological review. *Ecosphere* 9(1):e02088. 10.1002/ecs2.2088
- Howard, H., Watschke, T. 1991. Variable high-temperature tolerance among Kentucky Bluegrass cultivars. *Agronomy Journal*, 83, 689-693.
- Hu, Z., Yu, G., Zhou, Y., Sun, X., Li, Y., Shi, P., Wang, Y., Song, X., Zheng, Z., Zhang, L., Li, S. 2009. Partitioning of evapotranspiration and its controls in four grassland ecosystems: application of a two-source model. *Agricultural and Forest Meteorology*, 149, 1410-1420.
- Hui, D., Jackson, R. 2006. Geographical and interannual variability in biomass partitioning in grassland ecosystems: a synthesis of field data. *New Phytologist*, 169, 85–93.
- Ineson, P., Taylor, K., Harrison, A., Poskitt, J., Benham D., Tipping, E., Woof C. 1998. Effects of climate change on nitrogen dynamics in upland soils. 1. A transplant approach. *Global Change Biology*, 4, 143-152.
- Istanbulluoglu, E., Wang, T., Wedin, D. 2012. Evaluation of ecohydrologic model parsimony at local and regional scales in a semiarid grassland ecosystem. *Ecohydrology*, 5, 121-142.
- Jackson, R., Canadell, J., Ehleringer, J., Mooney, H., Sala, O., Schulze, E. 1996. A global analysis of root distributions for terrestrial biomes. *Oecologia*, 108, 389–411.
- Javaux, M., Couvreur, V., Vanderborght, J., Vereecken, H. 2013. Root water uptake: from three-dimensional biophysical processes to macroscopic modeling approaches. *Vadose Zone Journal*, doi:10.2136/vzj2013.02.0042
- Jarvis, N. 2011. Simple physics-based models of compensatory plant water uptake: concepts and ecohydrological consequences. *Hydrology and Earth System Sciences*, 15, 3431-3446.
- Jarvis, N., Koestel, J., Messing, I., Moeys, J., Lindahl, A. 2013. Influence of soil, land use and climatic factors on the hydraulic conductivity of soil. *Hydrology and Earth System Sciences*, 17, 5185-5195.
- Jenkinson, D., Potts, J., Perry, J., Barnett, V., Coleman, K., Johnston, A. 1994. Trends in herbage yields over the last century on the Rothamsted long-term continuous hay experiment. *Journal of Agricultural Science*, 122, 365-374
- Jing, Q., Bélanger, G., Baron, V., Bonesmo, H., Virkajärvi, P., Young, D. 2012. Regrowth simulation of the perennial grass timothy. *Ecological Modelling*, 232, 64-77.
- Johansson, G. 1993. Carbon distribution in grass (*Festuca pratensis* L.) during regrowth after cutting- utilization of stored and newly assimilated carbon. *Plant and Soil*, 151, 11-20.
- Jones, M., Leafe, E., Stiles, W. 1980a. Water stress in field-grown perennial ryegrass I. Its effect on growth, canopy photosynthesis, and transpiration. *Annals of Applied Biology*, 96, 87-101.
- Jones, M., Leafe, E., Stiles, W. 1980b. Water stress in field-grown perennial ryegrass I. Its effect on leaf water status, stomatal-resistance, and leaf morphology. *Annals of Applied Biology*, 96, 103-110.
- Jouven, M., Carrère, P., Baumont, R. 2006a. Model predicting dynamics of biomass, structure and digestibility of herbage in managed permanent pastures. 1. Model description. *Grass and Forage Science*, 61, 112–124.



- Jouven, M., Carrère, P., Baumont, R. 2006b. Model predicting dynamics of biomass, structure and digestibility of herbage in managed permanent pastures. 1. Model evaluation. *Grass and Forage Science*, 61, 125–133.
- Jupp, A., Newman, E. 1987. Morphological and anatomical effects of severe drought on the roots of *Lolium perenne* L. *New Phytologist*, 105, 393-402.
- Kahmen, A., Perner, J., Buchmann, N. 2005. Diversity-dependent productivity in semi-natural grasslands following climate perturbations. *Functional Ecology*, 19, 594-601.
- Katata, G., Grote, R., Mauder, M., Zeeman, M., Ota, M. 2020. Wintertime grassland dynamics may influence belowground biomass under climate change: a model analysis. *Biogeosciences*, 17, 1071-1085.
- Kellner, J., Multsch, S., Houska, T., Kraft, P., Müller, C., Breuer, L. 2017. A coupled hydrological-plant growth model for simulating the effect of elevated CO₂ on a temperate grassland. *Agricultural and Forest Meteorology*, 246, 42-50.
- Kemp, D., Culvenor, R. 1994. Improving the grazing and drought tolerance of temperate perennial grasses. *New Zealand Journal of Agricultural Research*, 37, 365-378.
- Kersebaum K., Hecker, J., Mirschel W., Wegehenkel M. 2007. Modelling water and nutrient dynamics in soil–crop systems: a comparison of simulation models applied on common data sets. In: Kersebaum, K., Hecker, J., Mirschel, W., Wegehenkel, M. (eds.) *Modelling water and nutrient dynamics in soil–crop systems*. Springer, Dordrecht.
- Kersebaum, K., Boote, K., Jorgenson, J., Nendel, C., Bindi, M., Frühauf, C., Gaiser, T., Hoogenboom, G., Kollas, C., Olesen, J., Rötter, R., Ruget, F., Thorburn, P., Trnka, M., Wegehenkel, M. 2015. Analysis and classification of data sets for calibration and validation of agro-ecosystem models. *Environmental Modelling and Software*, 72, 402-417.
- Kipling, R., Virkajärvi, P., Breitsameter, L., Curnel, Y., De Swaef, T., Gustavsson, A-M., Hennart, S., Höglind, M., Järvenranta, K., Minet, J., Nendel, C., Persson, T., Picon-Cochard, C., Rolinski, S., Sandars, D., Scollan N., Sebek, L., Seddaiu, G., Topp, C., Twardy, S., Van Middelkoop, J., Wu, L., Bellocchi, G. 2016. Key challenges and priorities for modelling European grasslands under climate change. *Science of the Total Environment*, 566–567, 851–864.
- Kirchner, J. 2006. Getting the right answers for the right reasons: linking measurements, analyses, and models to advance the science of hydrology. *Water Resources Research*, 42, W03S04, doi: <https://doi.org/10.1029/2005WR004362>.
- Klein, C., Biernath, C., Heinlein, F., Thieme, C., Gilgen, A., Zeeman, M., Priesack, E. 2017. Vegetation growth models improve surface layer flux simulations of a temperate grassland. *Vadose Zone Journal*, 16, doi:10.2136/vzj2017.03.0052
- Körner, C. 2008. Winter crop growth at low temperature may hold the answer for alpine treeline formation. *Plant Ecology and Diversity*, 1, 3-11.
- Körner, C. 2015. Paradigm shift in plant growth control. *Current Opinion in Plant Biology*, 25, 107–114.
- Kröbel, R., Sun, Q., Ingwersen, J., Chen, X., Zhang, F., Müller, T., Römheld, V. 2010. Modelling water dynamics with DNDC and DAISY in a soil of the North China Plain: a comparative study. *Environmental Modelling and Software*, 25, 583-601.



- Li, W., Ciais, P., Guenet, B., Peng, S., Chang, J., Chaplot, V., Khudyaev, S., Peregon, A., Piao, S., Wang, Y., Yue, C. 2018. Temporal response of soil organic carbon after grassland-related land-use change. *Global Change Biology*, 24, 4731-4746.
- Loka, D., Harper, J., Humphreys, M., Gasior, D., Wootton-Beard, P., Gwynn-Jones, D., Scullion, J., John Doonan, J., Kingston-Smith, A., Dodd, R., Wang, J., Chadwick, D., Hill, P., Jones, D., Mills, G., Hayes, F., Robinson, D. 2019. Impacts of abiotic stresses on the physiology and metabolism of cool-season grasses: a review. *Food and Energy Security*, 8:e00152.
- Luckner, L., van Genuchten, M., Nielsen, D. 1989. A consistent set of parametric models for the two-phase flow of immiscible fluids in the subsurface. *Water Resources Research*, 25, 2187–2193.
- Ma, S., Lardy, R., Graux, A-I., Ben Touhami, H., Klumpp, K., Martin, R., Bellocchi, G. 2015. Regional-scale analysis of carbon and water cycles on managed grassland systems. *Environmental Modelling and Software*, 72, 356-371.
- Manzoni, S., Vico, G., Porporato, A., Katul, G. 2013. Biological constraints on water transport in the soil–plant–atmosphere system. *Advances in Water Resources*, 51, 292-304.
- Martínez-Vilalta, J., Sala, A., Asensio, D., Galiano, L., Hoch, G., Palacio, S., Piper F., Lloret, F. 2016. Dynamics of non-structural carbohydrates in terrestrial plants: a global synthesis. *Ecological Monographs*, 86, 495-516.
- Maseda, P., Fernández, R. 2006. Stay wet or else: three ways in which plants can adjust hydraulically to their environment. *Journal of Experimental Botany*, 57, 3963-3977.
- Mboh, C., Srivastava, A., Gaiser, T., Ewert, F. 2019. Including root architecture in a crop model improves predictions of spring wheat grain yield and above-ground biomass under water limitations. *Journal of Agronomy and Crop Science*, 205, 109-128.
- Metselaar, K., Pinheiro, E., de Jong van Lier, Q. 2019. Mathematical description of rooting profiles of agricultural crops and its effect on transpiration prediction by a hydrological model. *Soil Systems*, 3, 44; doi:10.3390/soilsystems3030044.
- Meurer, K., Bolinder, M., Andren, O., Hansson, A-C., Pettersson, R., Kätterer, T. 2019. Shoot and root production in mixed grass ley under daily fertilization and irrigation: validating the N productivity concept under field conditions. *Nutrient Cycling in Agroecosystems*, 115, 85-99.
- Montaldo, N., Rondona, R., Albertson, J., Mancini, M. 2005. Parsimonious modeling of vegetation dynamics for ecohydrologic studies of water-limited ecosystems. *Water Resources Research*, 41, W10416, doi:10.1029/2005WR004094.
- Monteith, J. 1986. How do crops manipulate water supply and demand? *Philosophical transactions of the Royal Society of London A*, 316, 245-259.
- Monteith, J. 1988. Does transpiration limit the growth of vegetation or vice versa? *Journal of Hydrology*, 100, 57-68.
- Morvan-Bertrand, A., Pavis, N., Boucaud, J., Prud'homme M-P. 1999. Partitioning of reserve and newly assimilated carbon in roots and leaf tissues of *Lolium perenne* during regrowth after defoliation: assessment by ¹³C steady-state labelling and carbohydrate analysis. *Plant, Cell and Environment*, 22, 1097–1108.
- Mualem, Y. 1976. New model for predicting hydraulic conductivity of unsaturated porous-media. *Water Resources Research*, 12, 513-522.



- Nicotra, A., Davidson, A. 2010. Adaptive phenotypic plasticity and plant water use. *Functional Plant Biology*, 37, 117-127.
- Nicotra, A., Atkin, O., Bonser, S., Davidson, A., Finnegan, E., Mathesius, U., Poot, P., Purugganan, M., Richards, C., Valladares, F., van Kleunen, M. 2010. Plant phenotypic plasticity in a changing climate. *Trends in Plant Science*, 15, 684-692.
- Norris, I. 1982. Soil moisture and growth of contrasting varieties of *Lolium*, *Dactylis* and *Festuca* species. *Grass and Forage Science*, 37, 273-283.
- Nosalewicz, A., Siecińska, J., Kondracka, K., Nosalewicz, M. 2018. The functioning of *Festuca arundinacea* and *Lolium perenne* under drought is improved to a different extent by the previous exposure to water deficit. *Environmental and Experimental Botany*, 156, 271-278.
- Østrem, L., Rapacz, M., Jørgensen, M., Höglind, M. 2011. Effect of developmental stage on carbohydrate accumulation patterns during winter of timothy and perennial ryegrass. *Acta Agriculturae Scandinavica Section B – Soil and Plant Science*, 61, 153-163.
- Padilla, F., Aarts, B., Roijendijk, Y., de Caluwe, H., Mommer, L., Visser, E., de Kroon, H. 2013. Root plasticity maintains growth of temperate grassland species under pulsed water supply. *Plant Soil*, 369, 377-386.
- Persson, T., Höglind, M., Gustavsson, A-M., Halling, M., Jauhainen, L., Niemeläinen, O., Thorvaldsson, G., Virkajärvi, P. 2014. Evaluation of the LINGRA timothy model under Nordic conditions. *Field Crops Research*, 161, 87-97.
- Peters, A., Groh, J., Schrader, F., Durner, W., Vereecken, H., Pütz, T. 2017. Towards an unbiased filter routine to determine precipitation and evapotranspiration from high precision lysimeter measurements. *Journal of Hydrology*, 549, 731-740.
- Picon-Cochard, C., Pilon, R., Tarroux, E., Pagès, L., Robertson, J., Dawson, L. 2012. Effect of species, root branching order and season on the root traits of 13 perennial grass species. *Plant Soil*, 353, 47-57.
- Postma, J., Kuppe, C., Owen, M., Mellor, N., Griffiths, M., Bennett, M., Lynch, J., Watt, M. 2017. OPENSIMROOT: widening the scope and application of root architectural models. *New Phytologist*, 215, 1274-1286.
- Pütz, T., Kiese, R., Wollschläger, U., Groh, J., Rupp, H., Zacharias, S., Priesack, E., Gerke, H., Gasche, R., Bens, O., Borg, E., Baessler, C., Kaiser, K., Herbrich, M., Munch, J.-C., Sommer, M., Vogel, H.-J., Vanderborght, J., Vereecken, H. 2016. TERENO-SOILCan: a lysimeter-network in Germany observing soil processes and plant diversity influenced by climate change. *Environmental Earth Sciences*, 75, 1242.
- Raats, P. 2007. Uptake of water from soils by plant roots. *Transport in Porous Media*, 68, 5-28.
- Rahmati, M., Groh, J., Graf, A., Pütz, T., Vanderborght, J., Vereecken, H. 2020. On the impact of increasing drought on the relationship between soil water content and evapotranspiration of a grassland. *Vadoze Zone Journal*, doi: 10.1002/vzj2.20029.
- Robertson, M., Rebetzke, G., Norton, R. 2015. Assessing the place and role of crop simulation modelling in Australia. *Crop and Pasture Science*, 66, 877-893.



- Ruane, A., Phillips, M., Rosenzweig, C. 2018. Climate shifts within major agricultural seasons for +1.5 and +2.0°C worlds: HAPPI projections and AgMIP modeling scenarios. *Agricultural and Forest Meteorology*, 259, 329-344.
- Sándor, R., Barcza, Z., Acutis, M., Doro, L., Hidy, D., Köchy, M., Minet, J., Lellei-Kovács, E., Ma, S., Perego, A., Rolinski, S., Ruget, F., Sanna, M., Seddaiu, G., Wu, L., Bellocchi, G. 2017. Multi-model simulation of soil temperature, soil water content and biomass in Euro-Mediterranean grasslands: uncertainties and ensemble performance. *European Journal of Agronomy*, 88, 22-40.
- Schapendonk, A., Stol, W., van Kraalingen, D., Bouman, B. 1998. LINGRA, a sink/source model to simulate grassland productivity in Europe. *European Journal of Agronomy*, 9, 87-100.
- Schenk, H., Jackson, R. 2002. The global biogeography of roots. *Ecological Monographs*, 73, 311-328.
- Schmitt, A., Pausch, J., Kuzyakov, Y. 2013. Effect of clipping and shading on C allocation and fluxes in soil under ryegrass and alfalfa estimated by ¹⁴C labelling. *Applied Soil Ecology*, 64, 228-236.
- Schnepf, A., Leitner, D., Landl, M., Lobet, G., Mai, T-H., Morandage, S., Sheng, C., Zorner, M., Vanderborght, J., Vereecken, H. 2018. CRootBox: a structural-functional modelling framework for root systems. *Annals of Botany*, 121, 1033-1053.
- Seidel, S., Palosuo, T., Thorburn, P., Wallach, D. 2018. Towards improved calibration of crop models – where are we now and where should we go? *European Journal of Agronomy*, 94, 25-35.
- Shuttleworth, W., Wallace, J. 1985. Evaporation from sparse crops – an energy combination approach. *Quarterly Journal of the Royal Meteorological Society*, 111, 839-855.
- Shuttleworth, W., Gurney, R. 1990. The theoretical relationship between foliage temperature and canopy resistance in sparse crops. *Quarterly Journal of the Royal Meteorological Society*, 116, 497-519.
- Silvertown, J., Dodd, M., McConway, K., Potts, J., Crawley, M. 1994. Rainfall, biomass variation, and community composition in the Park Grass experiment. *Ecology*, 75, 2430-2437.
- Sinclair, T., Muchow, R. 1999. Radiation use efficiency. *Advances in Agronomy*, 65, 215-265
- Skinner, R., Comas, L. 2010. Root distribution of temperate forage species subjected to water and nitrogen stress. *Crop Science*, 50, 2178-2185.
- Smithwick, E., Lucash, M., McCormack, M., Sivandran, G. 2014. Improving the representation of roots in terrestrial models. *Ecological Modelling*, 291, 193-204.
- Staniak, M., Kocoń, A. 2015. Forage grasses under drought stress in conditions of Poland. *Acta Physiol. Plant.*, 37:116 DOI 10.1007/s11738-015-1864-1
- Stanimirova, R., Arévalo, P., Kaufmann, R., Maus, V., Lesiv, M., Havlík, P., Friedl, M. 2019. Sensitivity of global pasturelands to climate variation. *Earth's Future*, 7, 1353-1366.
- Stöckle, C., Kemanian, A. 2020. Can crop models identify critical gaps in genetics, environment, and management interactions? *Frontiers in Plant Science*, 11, 737. doi: 10.3389/fpls.2020.00737
- Sulis, M., Couvreur, V., Keune, J., Cai, G., Trebs, I., Junk, J., Shrestha, P., Simmer, C., Kollet, S., Vereecken, H., Vanderborght, J. 2019. Incorporating a root water uptake model based on the hydraulic architecture approach in terrestrial systems simulations. *Agricultural and Forest Meteorology*, 269-270, 28-45.



- Tardieu, F., Parent, B. 2017. Predictable ‘meta-mechanisms’ emerge from feedbacks between transpiration and plant growth and cannot be simply deduced from short-term mechanisms. *Plant, Cell and Environment*, 40, 846-857.
- Tardieu, F., Draye, X., Javaux, M. 2017. Root water uptake and ideotypes of the root system: whole-plant controls matter. *Vadose Zone Journal*, 16, doi:10.2136/vzj2017.05.0107
- Tardieu, F., Simonneau, T., Muller, B. 2018. The physiological basis of drought tolerance in crop plants: a scenario-dependent probabilistic approach. *Annual Reviews in Plant Biology*, 69, 733–759.
- Thomas, H. 1991. Accumulation and consumption of solutes in swards of *Lolium perenne* during drought and after rewatering. *New Phytologist*, 118, 35-48.
- Thomas, H., James, A. 1999. Partitioning of sugars in *Lolium perenne* (perennial ryegrass) during drought and on rewatering. *New Phytologist*, 142, 295-305.
- Tubiello, F., Soussana, J., Howden, S. 2007. Crop and pasture response to climate change. *Proceedings of the National Academy of Sciences of the USA*, 104, 19686–19690.
- van der Krift, T., Berendse, F. 2002. Root life spans of four grass species from habitats differing in nutrient availability. *Functional Ecology*, 16, 198-203.
- van Genuchten, M. 1980. A closed-form equation for predicting the hydraulic conductivity of unsaturated soils. *Soil Science Society of America Journal*, 44, 892–898.
- Vincent, C., Rowland, D., Schaffer, B., Bassil, E., Racette, K., Zurweller, B. 2020. Primed acclimation: a physiological process offers a strategy for more resilient and irrigation-efficient crop production. *Plant Science*, 295, 110240.
- Volaire, F., Thomas, H., Lelievre F., 1998. Survival and recovery of perennial forage grasses under prolonged Mediterranean drought I. Growth, death, water relations and solute content in herbage and stubble. *New Phytologist*, 140, 439-449.
- Wang, E., Smith, C. 2004. Modelling the growth and water uptake function of plant root systems: a review. *Australian Journal of Agricultural Research*, 55, 501-523.
- Wedderburn, M., Crush, J., Pengelly, W., Walcroft, J. 2010. Root growth patterns of perennial ryegrasses under well-watered and drought conditions. *New Zealand Journal of Agricultural Research*, 53, 377-388.
- Wegehenkel, M., Zhang, Y., Zenker, T., Diestel, H. 2008. The use of lysimeter data for the test of two soil–water balance models: a case study. *Journal of Plant Nutrition and Soil Science*, 171, 762-776.
- White, A., Rogers, A., Rees, M., Osborne, C. 2016. How can we make plants grow faster? A source-sink perspective on growth rate. *Journal of Experimental Botany*, 67, 31-45.
- Wingler, A. 2015. Comparison of signaling interactions determining annual and perennial plant growth in response to low temperature. *Frontiers in Plant Science*, 5, 794, doi: 10.3389/fpls.2014.00794.
- Wösten J., Lilly, A., Nemes, A., Le Bas, C. 1999. Development and use of a database of hydraulic properties of European soils. *Geoderma*, 90, 169-185.
- Wu, A., Song, Y., van Oosterom, E., Hammer, G. 2016. Connecting biochemical photosynthesis models with crop models to support crop improvement. *Frontiers in Plant Science* 7:1518. doi: 10.3389/fpls.2016.01518



- Zacharias, S., Bogen, H., Samaniego, L., Mauder, M., Fuß, R., Pütz, T., Frenzel, M., Schwank, M., Baessler, C., Butterbach-Bahl, K., Bens, O., Borg, E., Brauer, A., Dietrich, P., Hajsek, I., Helle, G., Kiese, R., Kunstmann, H., Klotz, S., Munch, J-C., Papen H., Priesack, E., Schmid, H-P., Steinbrecher, R., Rosenbaum, U., Teutsch, G., Vereecken, H. 2011. A network of terrestrial environmental observatories in Germany. *Vadose Zone Journal*, 10, 955-973.
- Zhang, L., Hu, Z., Fan, J., Zhou, D., Tang, F. 2014. A meta-analysis of the canopy light extinction coefficient in terrestrial ecosystems. *Frontiers in Earth Science*, 8, 599-609.
- Zhou, M., Ishidaira, H., Hapuarachchi, H., Magome, J., Kiem, A., Takeuchi, K. 2006. Estimating potential evapotranspiration using Shuttleworth–Wallace model and NOAA-AVHRR NDVI data to feed a distributed hydrological model over the Mekong River basin. *Journal of Hydrology*, 327, 151-173.
- Zwicke, M., Picon-Cochard, C., Morvan-Bertrand, A., Prud'homme, M-P., Volaire, F. 2015. What functional strategies drive drought survival and recovery of perennial species from upland grassland? *Annals of Botany*, 116, 1001-1015.



Table 1. Soil properties at Rollesbroich

Depth (cm)	Particle size distribution (%), fine earth fraction			Texture class (U.S.D.A.)	Organic carbon (%)	pH (CaCl ₂)
	Clay (<2 μm)	Silt (2-50 μm)	Sand (50-2000μm)			
0-7	19	14	67	Sandy loam	5.3	5.2
7-24	9	33	58	Sandy loam	2.5	5.3
24-42	37	23	40	Clay loam	1.2	5.4
42-50	35	33	32	Clay loam	0.8	5.4
50-71	32	32	36	Clay loam	0.3	5.4
71-93	32	32	36	Clay loam	0.3	5.2
93-127	17	24	59	Sandy loam	0.1	4.6
127+	22	30	48	Loam	0.2	4.9



Table 2. Measured water balance, harvested biomass and water use efficiency for the lysimeters (annual averages for the period 2013-2018; P = precipitation, PET = potential evapotranspiration calculated with the FAO Penman-Monteith method, AET = actual evapotranspiration, ΔS is the change of water storage calculated as P-AET-Percolation and WUE is water use efficiency defined as harvested biomass (Harvest) divided by AET).

Site	Lysimeter	P	PET	AET	Percolation	ΔS	Harvest	WUE
		[mm/year]				[g DM m ⁻² year ⁻¹]	[kg DM m ⁻³ water]	
Rollesbroich	Ro1	1055		649	438	-31	732	1.13
	Ro3	1079	710	651	466	-38	907	1.39
	Ro5	1050		623	422	5	678	1.09
	Average	1062		641	442	-21	772	1.20
Selhausen	Se21	696		716	-42	22	691	0.97
	Se25	690	827	709	-58	38	665	0.94
	Se26	699		714	-14	-1	661	0.93
	Average	695		713	-38	20	672	0.94



Table 3. Soil hydraulic parameters used in the modelling

Depths (cm)	Parameter					
	θ_s ($\text{m}^3 \text{m}^{-3}$)		α (cm^{-1})	n (-)	K_{10} (cm h^{-1})	τ (-)
	Selhausen	Rollesbroich				
0-24	0.45	0.55	0.025	1.34	1.89	0.5
24-48	0.39	0.39	0.025	1.09	0.73	0.5
48-90	0.38	0.38	0.025	1.08	0.83	0.5
90-140	0.38	0.38	0.025	1.17	1.46	0.5



Table 4. Fixed values for plant parameters at both sites

Parameter	Value	Sources/comments
Above-ground parameters		
Maximum radiation use efficiency, RUE_{max} ($\text{MJ m}^{-2} \text{d}^{-1}$)	1.6	¹ Akmal and Janssens (2004)
Leaf loss coefficient, k_{ag} (d^{-1})	0.02	Istanbulluoglu et al. (2012)
Specific leaf area, S_{leaf} ($\text{cm}^2 \text{g}^{-1}$)	142	Site data
Base temperature, T_b ($^{\circ}\text{C}$) for stomatal conductance and assimilation	0	² Wingler (2015), Körner (2008, 2015)
Base temperature, T_b ($^{\circ}\text{C}$) for DM allocation and leaf loss	5	² Schapendonk et al. (1998), Black et al. (2006), Hennessy et al. (2008)
Optimum temperatures, $T_{o(low)}$, $T_{o(high)}$ ($^{\circ}\text{C}$)	12, 25	Howard and Watschke (1991), Wu et al. (2016), Loka et al. (2019)
Ceiling temperature T_c ($^{\circ}\text{C}$)	35	Loka et al. (2019)
Limiting soil water pressure head for cessation of transpiration, ψ_w (m)	-150	Standard assumption
Fraction of assimilates allocated to roots under optimal conditions, $f_{bg(opt)}$ (-)	0.5	Hui and Jackson (2006)
Below-ground parameters		
Root decay constant, k_{bg} (d^{-1})	0.007	Van der Krift and Berendse (2002), Chen and Brassard (2013)
Root radius, r_o (cm)	0.02	Van der Krift and Berendse (2002), Picon-Cochard et al. (2012)
Effective root fraction, ε (-)	0.05	Faria et al. (2010)
Specific root length, S_{root} (m g^{-1})	118	Picon-Cochard et al. (2012)
Shape factor for root distribution, c (-)	-1.2	Schenk and Jackson (2002), Fan et al. (2016)

¹ assuming PAR = 50% of incoming solar radiation

² transpiration/assimilation is less sensitive to low temperatures than growth



Table 5. Uncertain parameters: initial ranges, data sources and post-priori parameter ranges

Parameter	Ranges sampled	Post-priori parameter values (n=30)					
		Selhausen			Rollesbroich		
		Median	Inter-quartile range	10 th , 90 th percentiles	Median	Inter-quartile range	10 th , 90 th percentiles
Radiation extinction coefficient, β	¹ 0.4-0.8	0.57	0.51-0.65	0.48, 0.71	0.58	0.51-0.65	0.48, 0.71
Maximum stomatal conductance, $k_{sto(max)}$ (cm s ⁻¹)	² 0.4-1.6	1.28	1.13-1.47	0.97, 1.56	0.60	0.48-0.83	0.46, 0.96
Maximum root depth, D_r (cm)	³ 40-100	79	75-83	70, 86	56	48-67	42, 73
Limiting pressure head at the root surface, $\psi_{o(crit)}$ (-cm)	⁴ 100-2000	271	233-347	195, 533	271	224-347	157, 419

¹ Schapendonk et al. (1998), Akmal and Janssens (2004), White and Snow (2012), Zhang et al. (2014)

² Nijs et al. (1997), Allen et al. (1998), Wang and Huang, (2003), DaCosta et al. (2004), Dong et al. (2011), Holloway-Phillips and Brodribb (2011), Hu et al., 2013

³ Site observations; Jackson et al. (1996), Schenk and Jackson (2002), Fan et al. (2016)

⁴ No information is available, hence a wide 'a priori' uncertainty range was selected



Table 6. Model efficiencies for the different data types (median values of the 30 acceptable parameter sets, with minimum and maximum values in parentheses).

Site	Model efficiency					
	Water content at 10cm depth	Water content at 30 cm depth	Water content at 50 cm depth	Evapo-transpiration	Harvest	Leaf area index
Ro	0.84 (0.78, 0.87)	0.77 (0.58, 0.83)	0.73 (0.64, 0.86)	0.58 (0.54, 0.60)	-0.70 (-0.54, -0.81)	0.19 (0.09, 0.50)
Se	0.81 (0.75, 0.84)	0.68 (0.58, 0.73)	0.28 (0.24, 0.31)	0.38 (0.32, 0.45)	0.35 (0.15, 0.46)	0.15 (-0.04, 0.32)

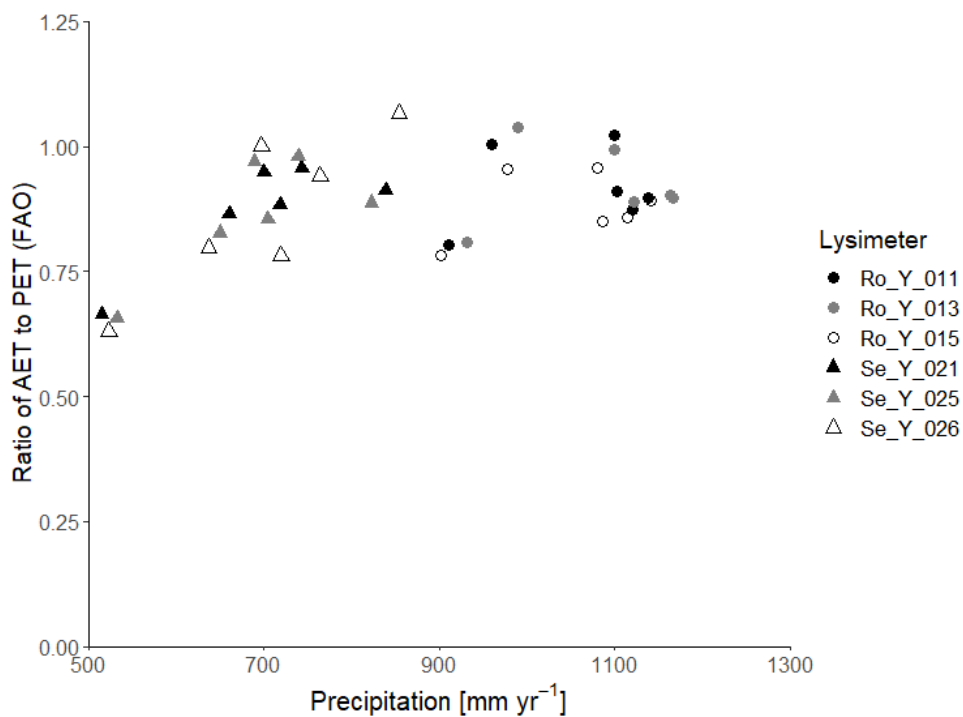


Figure 1. Ratio of actual evapotranspiration (AET) to potential evapotranspiration (PET-FAO) calculated with the FAO Penman-Monteith method (Allen et al., 1998) as a function of precipitation at Selhausen and Rollesbroich on an annual basis for the period 2013-2018.

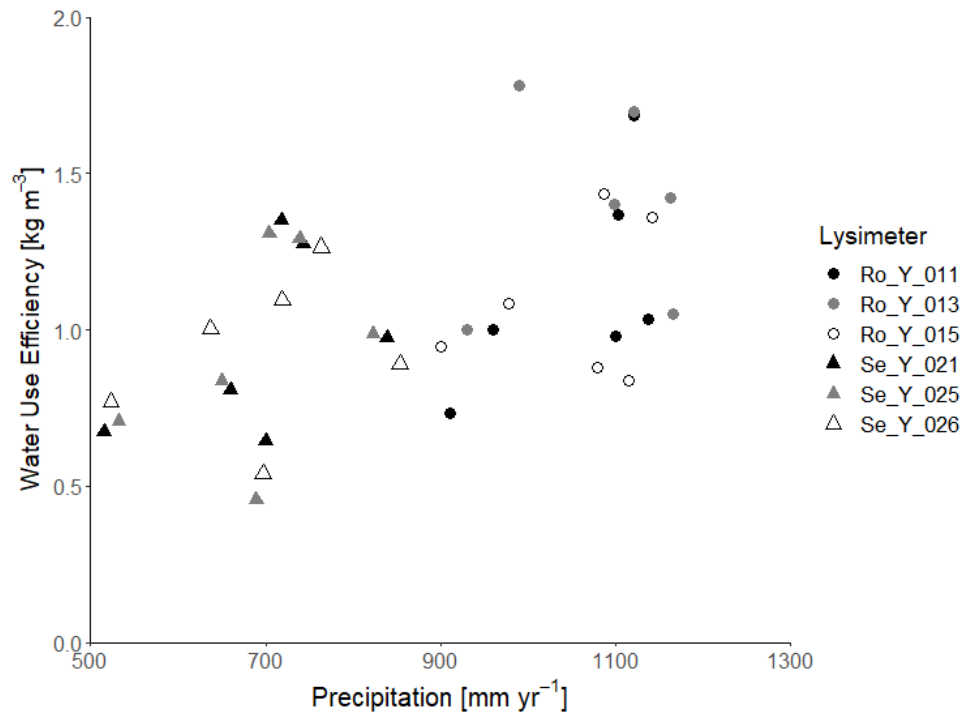


Figure 2. Water use efficiency (= annual harvest divided by annual evapotranspiration) as a function of annual precipitation at Selhausen and Rollesbroich.

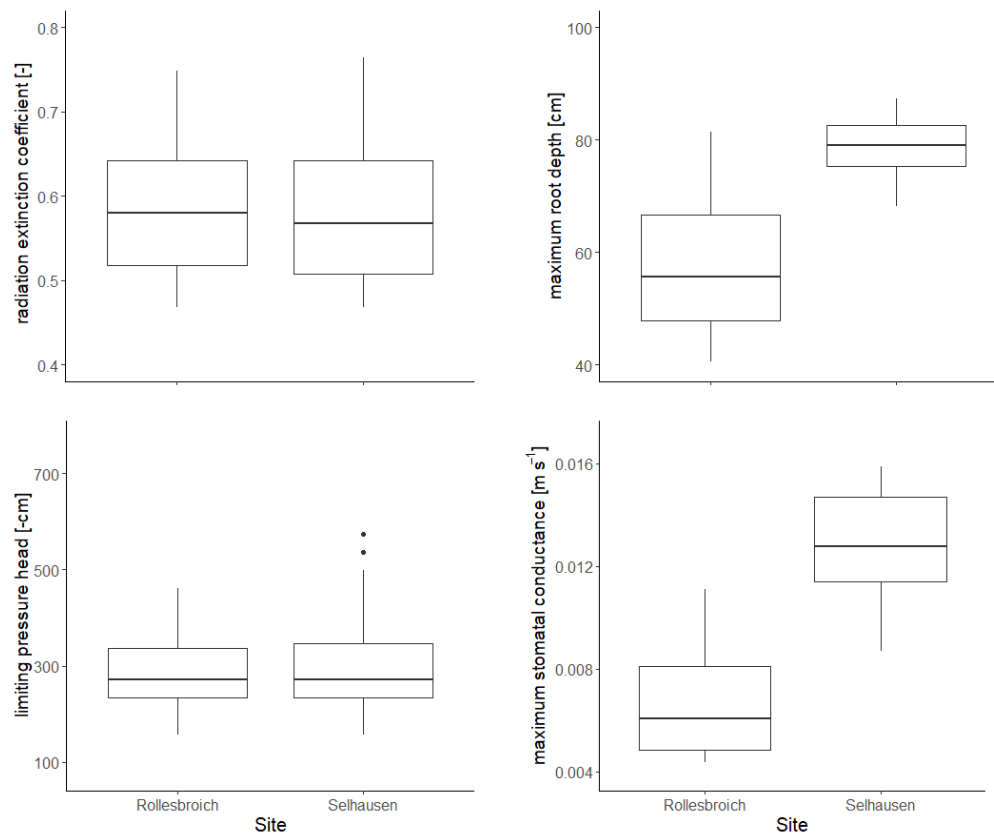


Figure 3. Posterior distributions of the four parameters treated as uncertain in the GLUE analysis. The horizontal line is the median value for the acceptable parameter sets, the box denotes 25th and 75th percentiles (inter-quartile range), the whiskers cover data points that lie within 1.5 times the inter-quartile range and solid circles represent outliers outside this range.

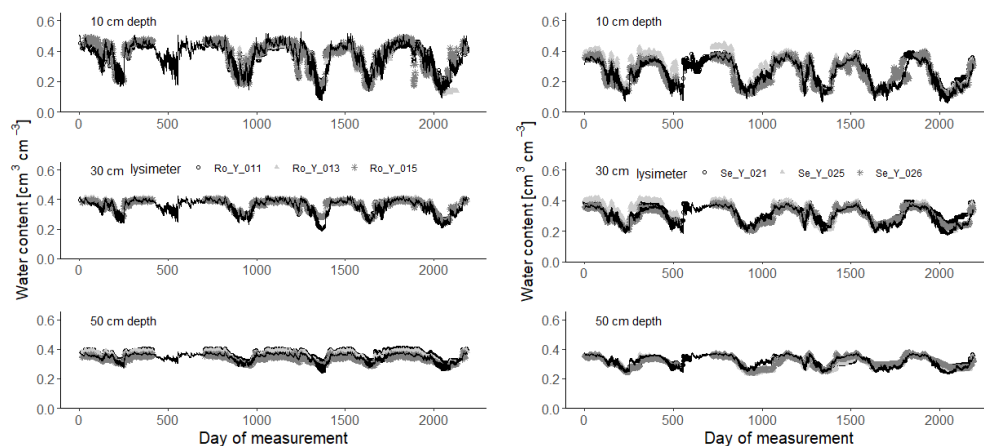


Figure 4. Measured soil water contents (symbols) at 10, 30 and 50 cm depth (2013-2018) compared with simulations for the 30 acceptable parameterizations at each site (black lines).

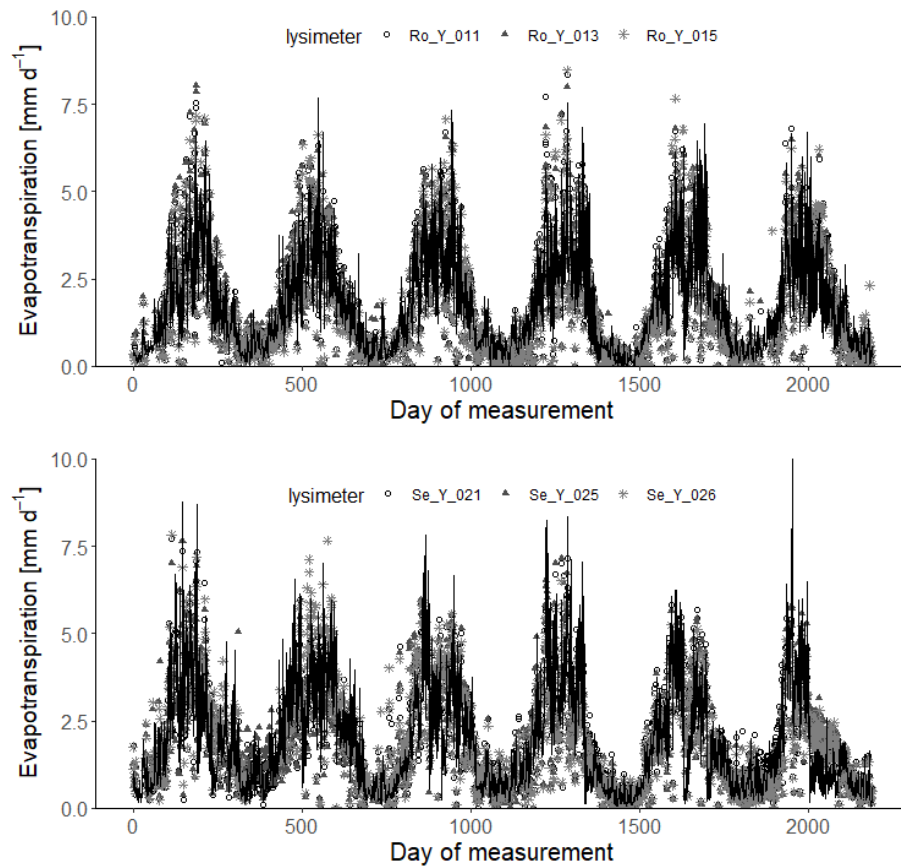


Figure 5. Measured daily evapotranspiration rates (symbols; 2013-2018) compared with simulations for the 30 acceptable parameterizations at each site (black lines).

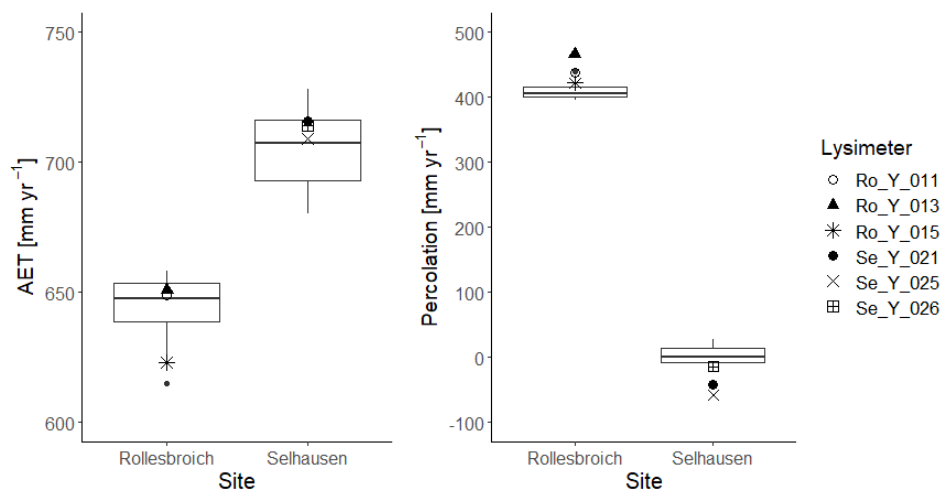


Figure 6. Box and whisker plots of simulated annual average evapotranspiration (AET) and percolation at Selhausen and Rollesbroich for the period 2013-2018 for the 30 acceptable simulations compared with the lysimeter measurements (large symbols). For an explanation of the box and whisker plots, see the caption to figure 3.

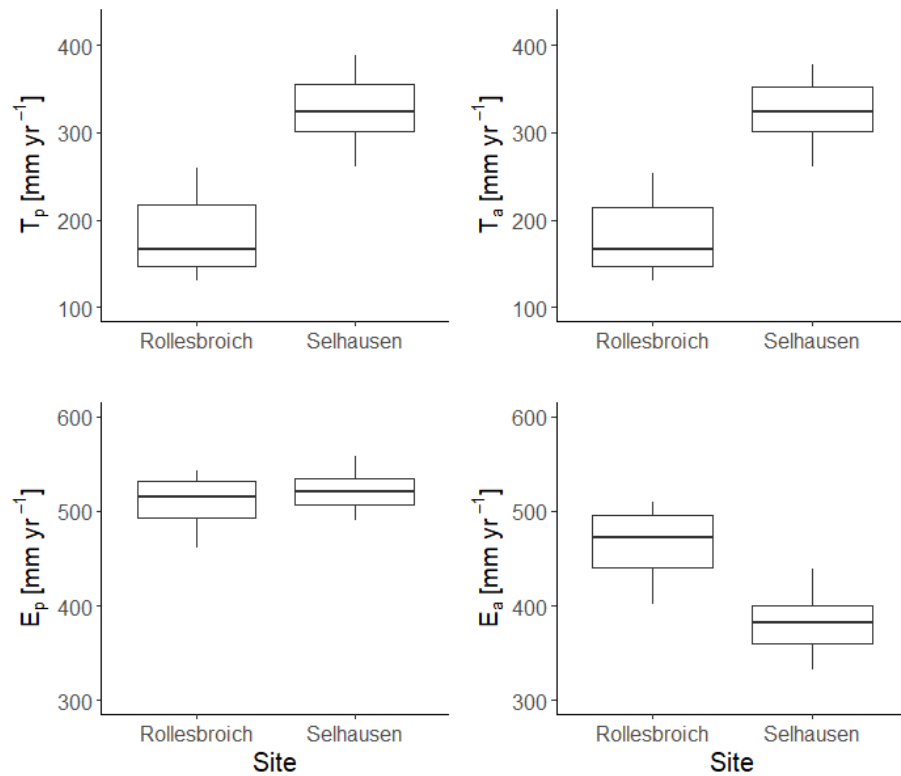


Figure 7. Simulated water balance terms for the 30 acceptable simulations at each site. For an explanation of the box and whisker plots, see the caption to figure 3.

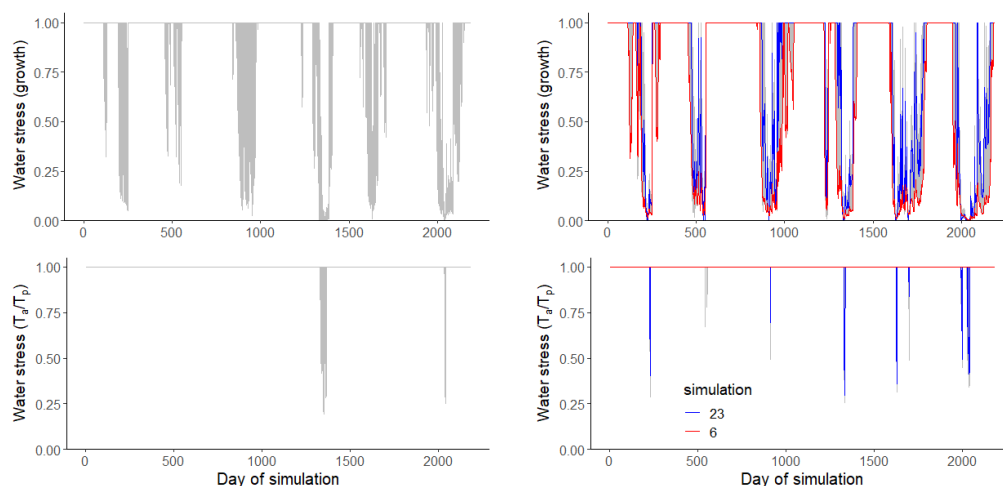


Figure 8. Plots of the two water stress functions in the model for the acceptable simulations. The uppermost figures show the threshold function of the pressure head at the root surface (equation 35) controlling dry matter allocation and leaf loss, while the figures at the bottom show the ratio of actual to potential transpiration, which controls assimilation (equation 34). Two contrasting acceptable simulations for the Selhausen site are highlighted in red and blue.

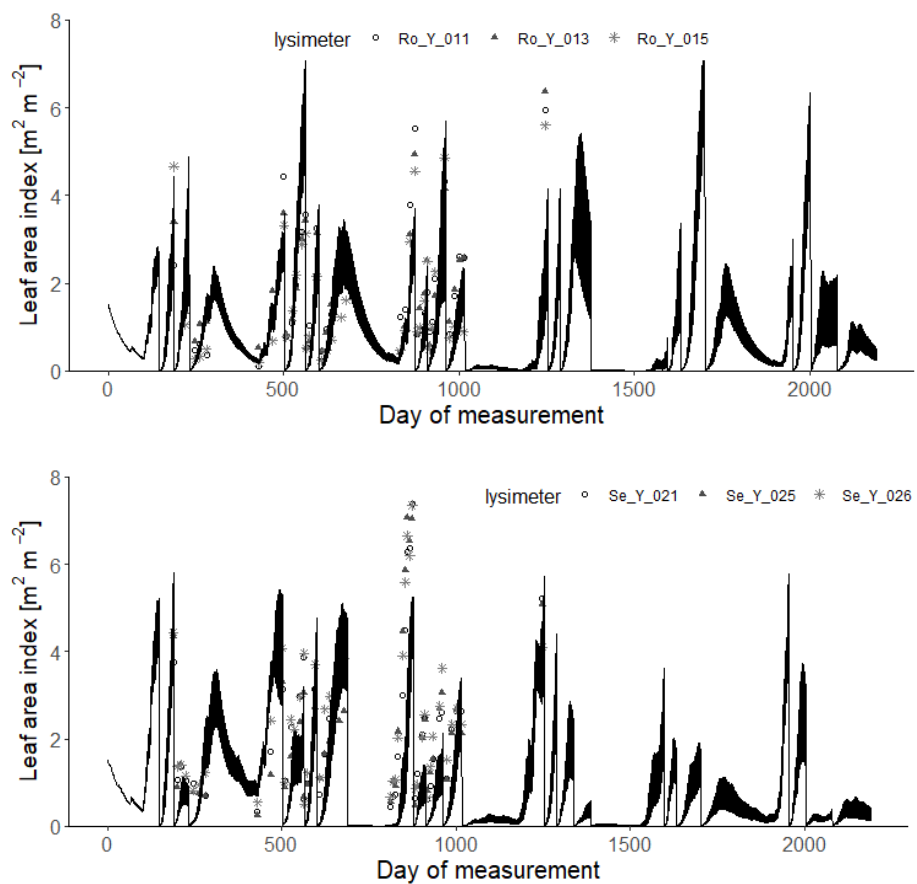


Figure 9. Measured daily leaf area index (symbols; 2013–2018) compared with simulations for the 30 acceptable parameterizations at each site (black lines).

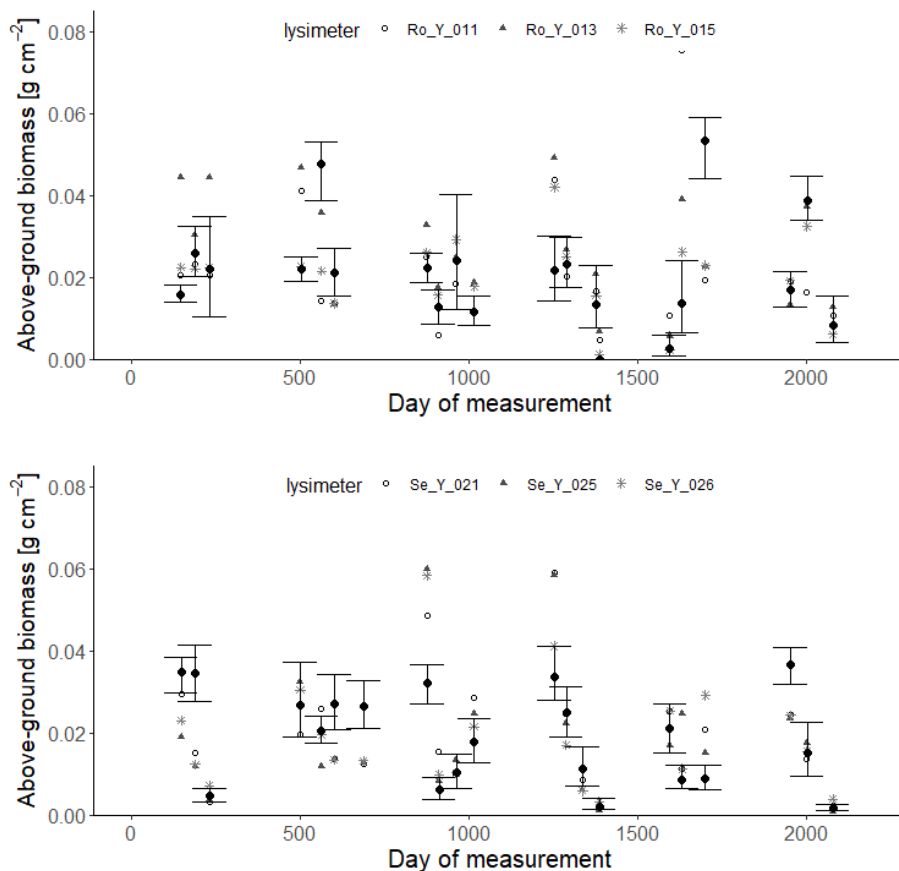


Figure 10. Measured harvests of above-ground biomass (symbols; 2013-2018) compared with simulations at each site (black symbols indicate means of the 30 acceptable parameterizations and the vertical lines denote minimum and maximum values).

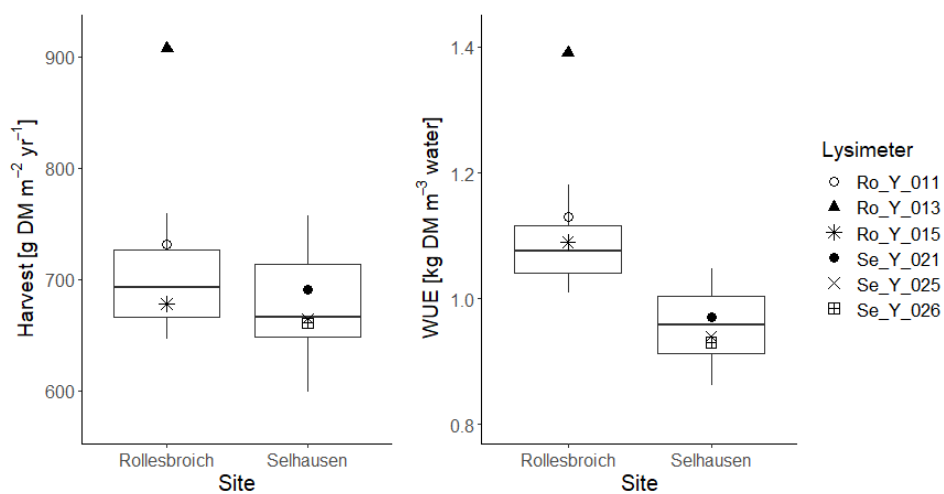


Figure 11. Box and whisker plots of simulated harvests and water use efficiencies (WUE, defined as total harvest divided by evapotranspiration) at Selhausen and Rollesbroich for the period 2013-2018 for the 30 acceptable simulations compared with lysimeter measurements (symbols). For an explanation of the box and whisker plots, see the caption to figure 3.

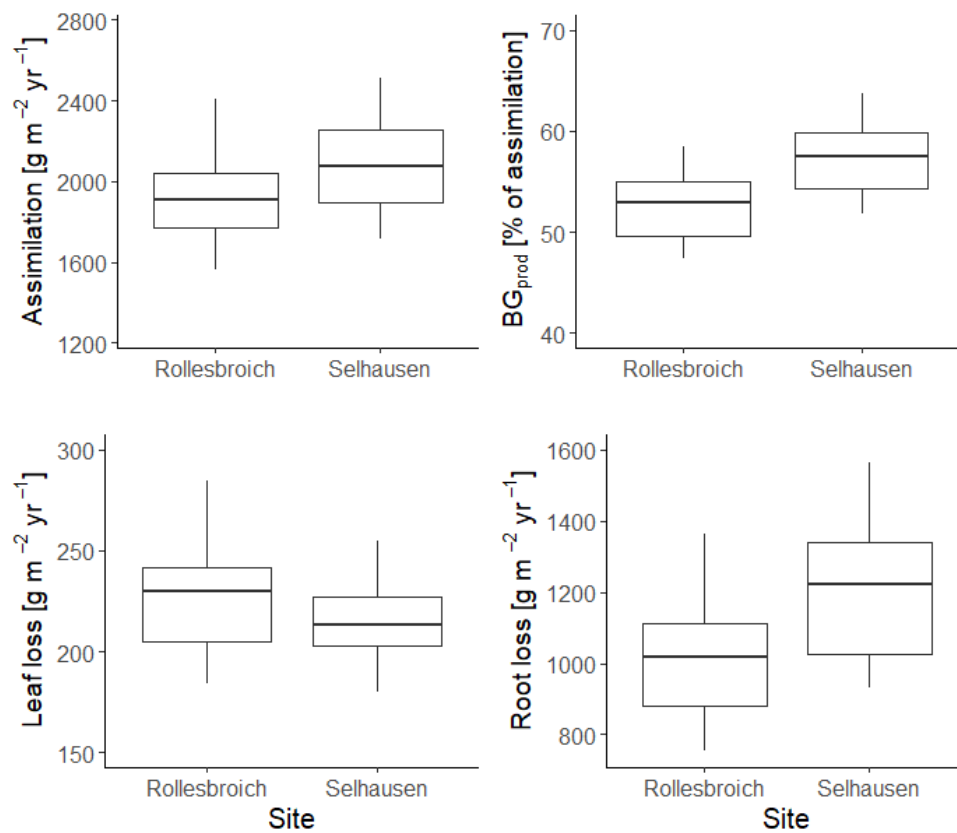


Figure 12. Box and whisker plots showing the simulated terms in the dry matter balance for the 30 acceptable model parameterizations at Selhausen and Rollesbroich for the period 2013-2018. For an explanation of the box and whisker plots, see the caption to figure 3.